BJP British Journal of Pharmacology

DOI:10.1111/bph.12830
www.brjpharmacol.org

RESEARCH PAPER

Conformational flexibility of the agonist binding jaw of the human P2X3 receptor is a prerequisite for channel opening

M Kowalski[1], R Hausmann[2], A Dopychai[2], M Grohmann[1,2], H Franke[1], K Nieber[3], G Schmalzing[2], P Illes[1] and T Riedel[1]

[1]*Rudolf-Boehm-Institute of Pharmacology and Toxicology, University of Leipzig, Leipzig, Germany,* [2]*Department of Molecular Pharmacology, RWTH Aachen University, Aachen, Germany, and* [3]*Department of Pharmacology for Natural Sciences, Institute of Pharmacy, University of Leipzig, Leipzig, Germany*

Correspondence
Maria Kowalski or Dr Peter Illes, Rudolf-Boehm-Institute of Pharmacology and Toxicology, University of Leipzig, Haertelstrasse 16-18, 04107 Leipzig, Germany. E-mail: maria.kowalski@medizin.uni-leipzig.de; peter.illes@medizin.uni-leipzig.de

Received
8 January 2014
Revised
16 June 2014
Accepted
19 June 2014

BACKGROUND AND PURPOSE

It is assumed that ATP induces closure of the binding jaw of ligand-gated P2X receptors, which eventually results in the opening of the membrane channel and the flux of cations. Immobilization by cysteine mutagenesis of the binding jaw inhibited ATP-induced current responses, but did not allow discrimination between disturbances of binding, gating, subunit assembly or trafficking to the plasma membrane.

EXPERIMENTAL APPROACH

A molecular model of the pain-relevant human (h)P2X3 receptor was used to identify amino acid pairs, which were located at the lips of the binding jaw and did not participate in agonist binding but strongly approached each other even in the absence of ATP.

KEY RESULTS

A series of cysteine double mutant hP2X3 receptors, expressed in HEK293 cells or *Xenopus laevis* oocytes, exhibited depressed current responses to α,β-methylene ATP (α,β-meATP) due to the formation of spontaneous inter-subunit disulfide bonds. Reducing these bonds with dithiothreitol reversed the blockade of the α,β-meATP transmembrane current. Amino-reactive fluorescence labelling of the His-tagged hP2X3 receptor and its mutants expressed in HEK293 or *X. laevis* oocytes demonstrated the formation of inter-subunit cross links in cysteine double mutants and, in addition, confirmed their correct trimeric assembly and cell surface expression.

CONCLUSIONS AND IMPLICATIONS

In conclusion, spontaneous tightening of the binding jaw of the hP2X3 receptor by inter-subunit cross-linking of cysteine residues substituted at positions not directly involved in agonist binding inhibited agonist-evoked currents without interfering with binding, subunit assembly or trafficking.

Abbreviations

α,β-meATP, α,β-methylene ATP; AA, amino acid; I_{max}, maximal current response; NBS, nucleotide binding segment; ORi, oocyte Ringer's solution; TEVC, two-electrode voltage-clamp; zf, zebrafish

Table of Links

TARGETS	LIGANDS
P2X3 receptor	ATP
P2Y receptors	

This Table lists key protein targets and ligands in this article which are hyperlinked to corresponding entries in http://www.guidetopharmacology.org, the common portal for data from the IUPHAR/BPS Guide to PHARMACOLOGY (Pawson *et al.*, 2014) and are permanently archived in the Concise Guide to PHARMACOLOGY 2013/14 (Alexander *et al.*, 2013a, b)

Introduction

Extracellular nucleotide receptors belong to the ionotropic P2X and metabotropic P2Y types (Abbracchio and Burnstock, 1994). P2X receptors are formed by a family of seven subunits, referred to as P2X1 through P2X7 (North, 2002; Kaczmarek-Hájek *et al.*, 2012; Khakh and North, 2012). These subunits consist of two transmembrane domains, a large extracellular loop contributing to the ATP binding site as well as intracellular N- and C-terminal tails. Early biochemical evidence indicated that homomeric receptors establish stable trimers of three identical subunits (Nicke *et al.*, 1998; Aschrafi *et al.*, 2004; Egan *et al.*, 2004).

In P2X receptors, three ATP binding sites exist at the interface of the extracellular loop of neighbouring subunits forming a jaw (Kawate *et al.*, 2009; Hattori and Gouaux, 2012; Jiang *et al.*, 2012). It is assumed that ATP induces closure of the binding jaw, which results in the opening of the membrane channel and the flux of mono- and divalent cations (Hattori and Gouaux, 2012; Jiang *et al.*, 2012; 2013). By generating double cysteine mutants of P2X subunits, the unrestricted movement of individual subunits relative to each other is inhibited, and in consequence, no gating of the receptor occurs after agonist binding. Because the largest conformational change of the receptor was found to take place adjacent to the ATP binding pouch in the extracellular domain, amino acid (AA) residues directly participating in agonist binding were replaced by cysteines, making it impossible to differentiate between the blockade of binding and gating (Marquez-Klaka *et al.*, 2007; Jiang *et al.*, 2011; Roberts *et al.*, 2012).

Homomeric, rapidly desensitizing P2X3 receptors are located at the peripheral terminals of pain-sensing dorsal root ganglion neurons and respond to ATP, which is released into the extracellular space as a noxious signalling molecule (Burnstock and Wood, 1996; Wirkner *et al.*, 2007). Previous mutagenesis studies identified the AA residues participating in agonist binding of hP2X3 receptors and generated a homology model of this receptor (Bodnar *et al.*, 2011). The aim of the present investigation was to systematically screen, by utilizing our homology model, AAs approaching each other near enough to form disulfide bonds, when cysteine residues were introduced at these critical positions. In such double mutant receptors, AAs located at the lips of the binding jaw (but not in the binding pouch itself) were replaced by cysteines; this leads to an immobilization of jaw movement by S–S bond formation, even without directly interfering with agonist binding, subunit assembly or trafficking to the plasma membrane. We suggest that spontaneous movements in the binding jaw may be promoted by ATP, which causes an 'induced-fit' allosteric change to reduce the energy barrier for gating and channel opening.

Methods

Homology model of hP2X3 receptor in the closed and open states

As previously described (Riedel *et al.*, 2012), we generated hP2X3 receptor models based upon the published closed (Kawate *et al.*, 2009) or open state (Hattori and Gouaux, 2012) zebrafish (zf)P2X4 crystal structure and the sequence of the hP2X3 receptor gene, with the loop model function of the Modeller 9v8 program (http://salilab.org/modeller), by using a standard script with improved loop refinement (Fiser and Sali, 2003).

Based upon the closed hP2X3 homology model, we simulated molecular dynamics with NAMD (http://www.ks.uiuc.edu/Research/namd) and visualized the receptor structure and dynamics with VMD (http://www.ks.uiuc.edu/Research/vmd). Within our molecular simulation, we could identify regions of the receptor ectodomain approaching each other around the agonist binding pouch. Based upon these findings, we planned potential cysteine double mutants enabling the formation of a disulfide bond (Supporting Information Fig. S1). To check the possibility of this disulfide bond formation, we generated once again homology models for the respective hP2X3 receptor cysteine double mutants with the Modeller 9v8 program. Then, we selected those cysteine double mutants, which exhibited the smallest molpdf energies and prepared the respective plasmids with site-directed mutagenesis. Subsequently, we compared the distances between the individual cysteine molecules at the backbone (C_α-carbons) of the closed and open state models of the receptor mutants and found them to be of similar magnitude (with the exception of K113/E270; Supporting Information Table S1), although the position of the relevant AA residues in the binding pouch, because of their unknown spatial orientation, might be somewhat different (Figure 1A–C, left panels; Supporting Information Fig. S2).

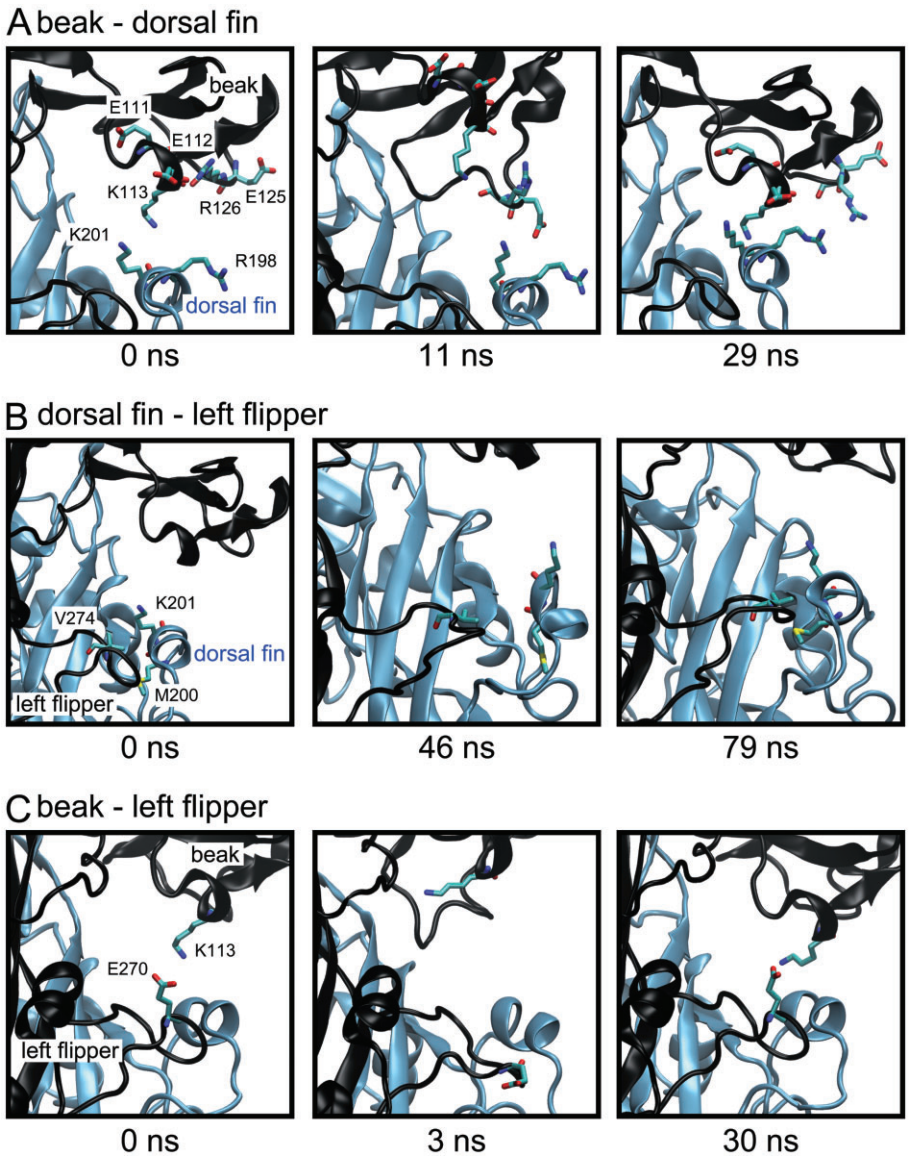

Figure 1

Homology model of the human (h)P2X3 receptor based upon the closed zebrafish (zf)P2X4R crystal structure. The generated 243 ns simulation of the molecular dynamics indicates a movement within the ectodomain near the ATP binding pouch, whereby domains of neighbouring receptor subunits (A and B) as well as intra-subunit domains (C) approach each other (boxed region of the receptor). Individual snapshots with cysteine mutagenesis-relevant AAs are shown at the time periods indicated (in nanoseconds): (A) The beak-dorsal fin interface is shown at three points of the simulation with beak residues Glu-111, Glu-112, Lys-113, Glu-125 and Arg-126 and the dorsal fin residues Arg-198 and Lys-201. (B) The dorsal fin-left flipper interface is shown at three points of the simulation with dorsal fin residues Met-200 and Lys-201 and the left flipper residue Val-274. (C) The beak-left flipper interface is shown at three points of the simulation with beak residue Lys-113 and left flipper residue Glu-270.

Site-directed mutagenesis

The pIRES2-EGFP plasmid carrying the hP2X3 receptor gene was utilized as the template for site-directed mutagenesis (Bodnar *et al.*, 2011). All cysteine single and double mutants of the hP2X3 receptor were generated by using the Quik-Change mutagenesis kit (Stratagene, La Jolla, CA, USA), and primers were synthesized by MWG Biotech (Ebersberg, Germany). The sequences were verified by IZKF (Leipzig, Germany).

Culturing of HEK293 cells and transfection procedures

HEK293 cells (Bodnar *et al.*, 2011) were kept in DMEM (PAA Laboratories, Cölbe, Germany) containing additionally 4.5 mg·mL^{-1} D-glucose, 10% FBS (both Invitrogen, Frankfurt, Germany) and 2 mM L-glutamine (Life Technologies, Frankfurt, Germany) at 37°C and 5% CO_2 in humidified air. For electrophysiology, HEK293 cells were plated in plastic dishes 6 h before transient transfection. Further, 0.5 μg of plasmid

DNA, 10 µL of PolyFect reagent (Qiagen, Hilden, Germany) and 100 µL of OptiMEM (Life Technologies) were combined and incubated for 10 min, before introduction of lipid-DNA complexes to HEK293 cells. About 18 h after transfection, the medium was replaced by OptiMEM for removing residual plasmid DNA.

Whole-cell patch clamp recordings

Whole-cell patch clamp recordings were performed 2–4 days after transient transfection of HEK293 cells, at room temperature (20–22°C), using an Axopatch 200 B patch clamp amplifier (Molecular Devices, Sunnyvale, CA, USA). The pipette solution contained (in mM) CsCl 135, $MgCl_2$ 2, HEPES 20, EGTA 11, $CaCl_2$ 1, Mg-ATP 1.5 and Li-GTP 0.3; pH adjusted to 7.4 using CsOH. The external physiological solution contained (in mM) NaCl 135, KCl 5, $MgCl_2$ 2, $CaCl_2$ 2, HEPES 10 and D-glucose 11; pH adjusted to 7.4 using NaOH.

The pipette resistances varied between 3 and 7 MΩ. The liquid junction potential (V_{LJ}) between the bath and pipette solution at 21°C was calculated to be −4.5 mV. Holding potential values given in this study were corrected for V_{LJ}. All recordings were carried out at a holding potential of −65 mV. Data were filtered at 2 kHz with the inbuilt filter of the amplifier, digitized at 5 kHz and stored on a laboratory computer using a Digidata 1440 interface and pClamp 10.2 software (Molecular Devices).

Drugs were dissolved in the external solution and locally superfused to single cells using a rapid solution exchange system (SF-77B Perfusion Fast-Step; Warner Instruments, Hamden, CT, USA). The receptor functionality was tested by applying increasing concentrations (0.3–300 µM) of the P2X1,3-selective agonist α,β-methylene ATP (α,β-meATP) for 2 s at an interval of 5 min. The amplitudes of the agonist-induced currents were plotted as concentration–response curves.

For testing the reversibility of disulfide bond formation, a standard concentration of α,β-meATP (10 µM; Tocris, Bristol, UK) was applied for 2 s at an interval of 5 min, eight times in total. After 10 min (two agonist applications), the reducing reagent DTT (1 mM; Sigma-Aldrich, Steinheim, Germany) was superfused for 15 min (three agonist applications), followed by a washout period with external solution for additional 15 min (three agonist applications). In a few cases, DTT was superfused for 20 min, and after the third application of α,β-meATP, only the external solution was superfused for 2 s with the rapid application system; then, we followed the regular superfusion protocol.

Biochemical analysis of receptor oligomerization and cell surface expression in HEK293 cells

The coding region of the N-terminally hexahistidine-tagged (His-tagged) hP2X3 subunit His-hP2X3 and the derived cysteine double mutants were subcloned into the pcDNA5/FRT/TO inducible expression vector using the Gateway cloning system, following the manufacturer's instructions (Life Technologies), to generate stable Flp-In HEK293 cell lines. The stable cell lines were cultured at 37°C in DMEM (Life Technologies) supplemented with 10% FCS (PAA Laboratories), 100 U·mL^{-1} of penicillin G and 100 µg·mL^{-1} of streptomycin. After plating each cell line into one 30 mm well, expression was induced by 1 µg·mL^{-1} of tetracycline for 36 h. After carefully washing the cells with HBSS containing calcium and magnesium but no phenol red (Life Technologies) to remove the cell culture medium including the FCS completely, the cells were surface labelled with IRDye® 800CX NHS ester (80 µg·mL^{-1}) (Li-Cor Biosciences, Bad Homburg, Germany) for 30 min at 37°C. After washing the cells with HBSS, proteins were solubilized with dodecylmaltoside (DDM, 0.2%, w/v) in PBS, pH 8.0. The His-hP2X3 proteins were purified by Ni-NTA affinity chromatography under non-denaturing conditions, washed, eluted in imidazole/0.02% DDM buffer and subjected to SDS-PAGE and blue native PAGE (BN-PAGE) as previously described (Nicke *et al.*, 1998; Aschrafi *et al.*, 2004; Fallah *et al.*, 2011; Hausmann *et al.*, 2012).

Expression of the hP2X3 receptor and its mutants in X. laevis oocytes

An oocyte expression plasmid harbouring the cDNA for His-tagged hP2X3 subunit has been previously described (Bodnar *et al.*, 2011; Hausmann *et al.*, 2012). Replacement mutations were introduced by QuikChange site-directed mutagenesis (Stratagene) and verified by sequencing (MWG Biotech). Capped cRNAs were synthesized and injected in aliquots of 46 nL (0.8–1.3 ng·nL^{-1}) into collagenase-defolliculated *X. laevis* oocytes using a Nanoliter 2000 injector (World Precision Instruments, Berlin, Germany) as previously described (Hausmann *et al.*, 2006). Oocytes were cultured at 19°C in sterile oocyte Ringer's solution (ORi; in mM): NaCl 90, KCl 1, $CaCl_2$ 1, $MgCl_2$ 1 and HEPES 10; pH 7.4) supplemented with 50 µg·mL^{-1} of gentamycin.

Two-electrode voltage-clamp (TVEC) electrophysiology

One to two days after cRNA injection, current responses were evoked by α,β-meATP, as indicated at ambient temperature (21–24°C), and recorded by conventional TEVC in Mg-ORi solution (Mg-ORi; in mM): NaCl 90, KCl 1, $MgCl_2$ 2 and HEPES 10; pH 7.4) with a Turbo TEC-05 amplifier (npi Electronics, Tamm, Germany) at a holding potential of −60 mV as previously described (Hausmann *et al.*, 2006). For testing the reversibility of disulfide bond formation, P2X3 receptor-mediated currents were elicited in 5 min intervals by 10 s lasting applications of 10 µM α,β-meATP. Between the α,β-meATP applications, the oocytes were superfused with Mg-ORi. Following two such cycles of hP2X3 receptor activation, three further cycles of activation were performed under reducing conditions with 1 mM DTT present in both solutions, Mg-ORi with and without α,β-meATP. The final three cycles of activation were performed in the absence of DTT, that is, exactly as the two initial cycles.

Biochemical analysis of receptor oligomerization and cell surface expression in X. laevis oocytes

cRNA-injected oocytes were metabolically labelled and surface labelled as previously described (Fallah *et al.*, 2011; Hausmann *et al.*, 2012), with the exception that the membrane-impermeant infrared dye IRDye 800CX NHS ester

(Li-Cor Biosciences) was used for surface labelling at a final concentration of 100 μg·mL^{-1} (diluted 200-fold from a stock solution in dimethyl sulfoxide). His-tagged proteins were purified by non-denaturing Ni-NTA chromatography (Qiagen) from digitonin (1%, w/v) extracts of the oocytes and released in the non-denatured state from the Ni-NTA sepharose. The proteins were analysed by BN-PAGE or SDS-PAGE in the non-denatured or SDS-denatured state, respectively, as previously described (Fallah *et al.*, 2011; Hausmann *et al.*, 2012). The IRDye 800CX-labelled plasma membrane-bound proteins were visualized with the Odyssey fluorescence scanner (Li-Cor Biosciences).

The intensity of the fluorescent protein bands was quantified using the ImageQuant TL software version 7.0 (GE Healthcare, Freiburg, Germany). Images of PAGE gels were prepared with Image-Quant TL for contrast adjustments. If necessary, individual lanes from PAGE gels were differently enhanced by the ImageQuant software for better visibility of weak and strong protein bands. The image sections were cropped and positioned using Adobe Photoshop CS5. Microsoft PowerPoint 2010 was used for labelling. Each experiment was performed at least twice with equivalent results.

Visualization of agonist binding using BODIPY ATP

X. laevis oocytes, injected with cRNA for wild-type (wt) hP2X3 or its mutants K113C/K201C, M200C/V274C and K201C/V274C, were transferred to a bath chamber and incubated with 0.1 μM of the fluorescent agonist BODIPY-TR ATP (BODIPY ATP; Invitrogen), which exhibits spectral properties similar to the fluorescent dye Texas Red, dissolved in Mg-ORi. The agonist binding to the wt hP2X3 receptor and its mutants on the oocyte surface was visualized with a laser scanning microscope (LSM 510; Carl Zeiss, Oberkochen, Germany). Confocal images were collected every minute for 24 min (see Figure 6D–H). BODIPY ATP was added to the bath 1 min after starting the experiment at time 0. After 9 min of incubation with BODIPY ATP, 1 mM DTT was additionally applied. The specific binding of BODIPY ATP to the cell surface was calculated as the difference of the fluorescence intensity at the cell membrane and the cytoplasm, measured over the entire incubation period. Data were normalized to the fluorescence intensity measured at time 0 min and are expressed in relative fluorescence units. To show that bound BODIPY ATP (0.1 μM) can be specifically displaced from the hP2X3 receptor at the cell surface, oocytes were pre-incubated with 0.1 μM BODIPY ATP alone before 30 μM α,ß-meATP was added in the continuous presence of 0.1 μM BODIPY ATP. The subsequent decay of plasma membrane-bound fluorescence was recorded for 15 min.

Data analysis

The agonist concentration–response curves were fitted using the three parametric Hill equation:

$$I = I_{max} \cdot [A^{n_H}/(EC_{50}{}^{n_H} + [x^{n_H}])]$$

where I is defined as the peak current evoked by α,β-meATP concentration [A], I_{max} is the peak current evoked by a maximal α,β-meATP concentration, EC_{50} is the half-maximal effective concentration and n_H is the Hill coefficient (Origin 8.0; OriginLab, Northampton, MA, USA). The data are presented as means ± SEM of n experiments. For comparing the effects of α,β-meATP at the cysteine double mutants with effects at the respective cysteine single mutants, and effects at the double/single mutants with that at the wt hP2X3 receptor, a one-way ANOVA followed by the Holm–Sidak *post hoc* test was used. The effect of DTT was evaluated by ANOVA followed by the Bonferroni *post hoc* test for repeated measures. A probability level of 0.05 or less was considered to reflect a statistically significant difference.

Results

Homology model and molecular dynamics simulation of ectodomain movements of the hP2X3 receptor

The P2X subunit resembles the shape of a dolphin, with the transmembrane helices and the extracellular region akin to the flukes and the upper body respectively (Kawate *et al.*, 2009). Attached to the body domain are the head domain and three structurally different elements: the dorsal fin, the right flipper and the left flipper (Supporting Information Fig. S1). We asked ourselves whether ATP binding could be altered by selective tightening of the agonist binding pouch and the consequent immobilization of the P2X3 receptor structure. The homology model of the hP2X3 receptor in conjunction with molecular dynamics simulation indicates a highly flexible extracellular loop associated with movements within this ectodomain near the ATP binding sites in the nanosecond range (Figure 1). We identified movements in the receptor, on the one hand, where beak and dorsal fin (Figure 1A) as well as left flipper and dorsal fin (Figure 1B) of different subunits approached each other, and on the other hand, where beak and left flipper of the same subunit converged (Figure 1C).

We assume from our molecular dynamics simulation the existence of hydrogen bonds and salt bridges between adjacent receptor subunits. By introducing two opposing cysteine residues at the assumed contact sites, a disulfide bond was created to immobilize the receptor in one state of operation (either open or closed conformation). Based upon the hP2X3 model, we have chosen pairs of cysteine mutants at certain sites of the receptor ectodomain which might allow the formation of inter- or intra-subunit disulfide bonds. While the first set of mutants was designed to cross-link beak (E111, E112, K113, E125, R126) and dorsal fin (R198, K201; Supporting Information Fig. S1C, panel a) of adjacent subunits, the second set of mutants should cross-link left flipper (V274) and dorsal fin (M200, K201; Supporting Information Fig. S1C, panel b) of neighbouring subunits. Furthermore, we generated a cysteine double mutant enabling the formation of an intra-subunit disulfide bond between beak (K113) and left flipper (E270; Supporting Information Fig. S1C, panel c).

Measurement of receptor function by whole-cell patch clamp recordings in hP2X3-HEK293 cells

The wt hP2X3 receptor and its cysteine mutants and double mutants were transiently expressed in HEK293 cells. The influence of the inserted cysteine residues, and a potentially

formed disulfide bond between opposing cysteines, on the functional consequences of ATP binding and/or conformational changes required for pore opening was measured by the whole-cell patch clamp technique using the P2X1,3-selective agonist α,β-meATP (0.3–300 μM; Figure 2A).

Concentration–response curves for α,β-meATP were generated at wt hP2X3 and its cysteine single and double mutants. The EC_{50} of α,β-meATP, the maximal attainable current (I_{max}), as well as n_H are presented in Table 1. Whereas the function of the hP2X3 cysteine single mutants was usually only slightly inhibited in comparison with that of the wt receptor (Figure 2B,C,F,G; Table 1), the function of the cysteine double mutants was more markedly depressed (Figure 2D–G; Table 1). Within each set of cysteine double mutants forming a putative inter-subunit disulfide bond either between beak-dorsal fin and left flipper-dorsal fin of two adjacent subunits, K113C/K201C (Figure 2D) and M200C/V274C or K201C/V274C (Figure 2F), respectively, responded to α,β-meATP with very small current amplitudes. By contrast, the function of the hP2X3 cysteine double mutant, forming an intra-subunit disulfide bond between beak and left flipper (K113C/E270C), was less markedly suppressed (Figure 2G).

Reversibility of disulfide bond formation

For restoring the mobility of hP2X3 receptor cysteine double mutants, the reducing reagent DTT was applied to break up disulfide bonds (for the standard application protocol, see Figure 3A). DTT (1 mM) did not alter the amplitudes of the α,β-meATP (10 μM)-induced currents at the wt hP2X3 receptor or any of its mutants, where a single cysteine residue replaced the previously selected AAs (Figure 3A and C). However, DTT moderately increased the small current responses to α,β-meATP (10 μM) at the double cysteine mutants E111C/K201C, E112C/R198C, K113C/R198C, E125C/R198C and R126C/K201C; a large (from 9- to 24-fold) increase of the current amplitude occurred with the mutants K113C/K201C and K201C/V274C in the presence of DTT. After washing out DTT for 15 min, the currents declined to their original level, suggesting spontaneous reoxidation of the thiols (Figure 3A and C). We demonstrated in a few experiments that both the application of H_2O_2 and the washout of DTT by normal extracellular medium causes a reoxidation of the thiols, resulting in decreased currents (Figure 3B; cf. Marquez-Klaka *et al.*, 2007; Liang *et al.*, 2013).

Figure 3C–E shows the statistical evaluation of all experiments on a percentage basis; as mentioned in the Methods section, data were normalized with respect to the pre-DTT amplitude of the α,β-meATP currents. It became clear that there was no potentiation by DTT at the M200C/V274C double mutant, in spite of the very small control α,β-meATP currents observed (compared with the much larger current amplitudes at the wt hP2X3 receptor) (Figures 2F and 3A). Moreover, DTT had no effect on the residual series of double mutants E111C/R198C, E112C/K201C, E125C/HK201C and R126C/R198C either (Figure 3D). The K113C/E270C intra-subunit cysteine mutation depressed the α,β-meATP-induced current amplitude compared with wt, but did not change its EC_{50} value (Figure 2G; Table 1). The decrease in the current response did not recover after DTT application (Figure 3D). The reason for this finding may be that either no S–S bond was created or that the newly formed S–S bond did not hinder the conformational change during the activation process. Thus, we did not consider these latter AA residues of significance for channel gating.

It was an unexpected finding that DTT strongly rescued the effect of α,β-meATP at K201C/V274C-hP2X3, but not at the M200C/V274C-hP2X3 in its immediate neighbourhood. Molecular models of M200C/V274C and K201C/V274C cross-linking left flipper and dorsal fin of adjacent receptor subunits suggested that the disulfide bond might not be accessible to DTT in case of the M200C/V274C mutation (compare Supporting Information Fig. S3A, panels a, c with panel b).

In the following experiments, we selected those double mutants at which the effect of α,β-meATP (10 μM) was potentiated by DTT in a statistically significant manner (Figure 3E). To find out whether DTT also increases the current amplitudes elicited by a higher concentration of α,β-meATP (100 μM), a similar application protocol was used as shown in Figure 3A. Under these conditions, the DTT effect was lost at E111C/K201C, E125C/R198C and R126C/K201C, but otherwise remained basically unchanged at the mutants tested with α,β-meATP (10 μM) (Figure 3E).

Then, we established concentration–response curves for α,β-meATP (0.3–300 μM) at HEK293 cells transfected with the wt hP2X3 receptor or its cysteine double mutants K113C/K201C and K201C/V274C in the absence and presence of 1 mM DTT (Figure 3F, panels a and b). According to our expectations, DTT neither altered the EC_{50} and I_{max} values nor the n_H for α,β-meATP at the wt receptors, when compared

Figure 2

Current responses to α,β-methylene ATP (α,β-meATP) in HEK293 cells transfected with the wt hP2X3 receptors and its cysteine single or double mutants. Increasing concentrations of α,β-meATP (0.3–300 μM) were applied locally for 2 s with 5 min intervals at a holding potential of –65 mV. (A) Rapidly activating and desensitizing inward current responses of the wt hP2X3 receptor. Numbers between the current traces indicate the time (in min) which elapsed between agonist application. (B, C) Concentration–response curves for α,β-meATP at the wt hP2X3 receptor as well as the first (B) and second (C) set of its cysteine single mutants, where the mutations are located at the beak and dorsal fin of this dolphin-like structure. (D, E) Concentration–response curves for α,β-meATP at the wt hP2X3 receptor and the first (D) and second (E) set of its cysteine double mutants supposedly linking the beak and dorsal fin of this dolphin-like structure. (F) Concentration–response curves for α,β-meATP at the wt hP2X3 receptor and its single mutants, where the mutations are situated at the dorsal fin and left flipper of this dolphin-like structure, and the respective double mutants supposedly linking the respective AAs in two adjacent subunits. (G) Concentration–response curves for α,β-meATP at the wt hP2X3 receptor and its single mutants situated at the beak and left flipper of this dolphin-like structure, and the respective double mutants supposedly linking the respective AAs in a subunit. Maximal current responses through the double mutant receptors were usually smaller than those through the respective two individual single mutant receptors (see I_{max} values in Table 1). Each symbol indicates the mean ± SEM of 6–8 cells, as indicated.

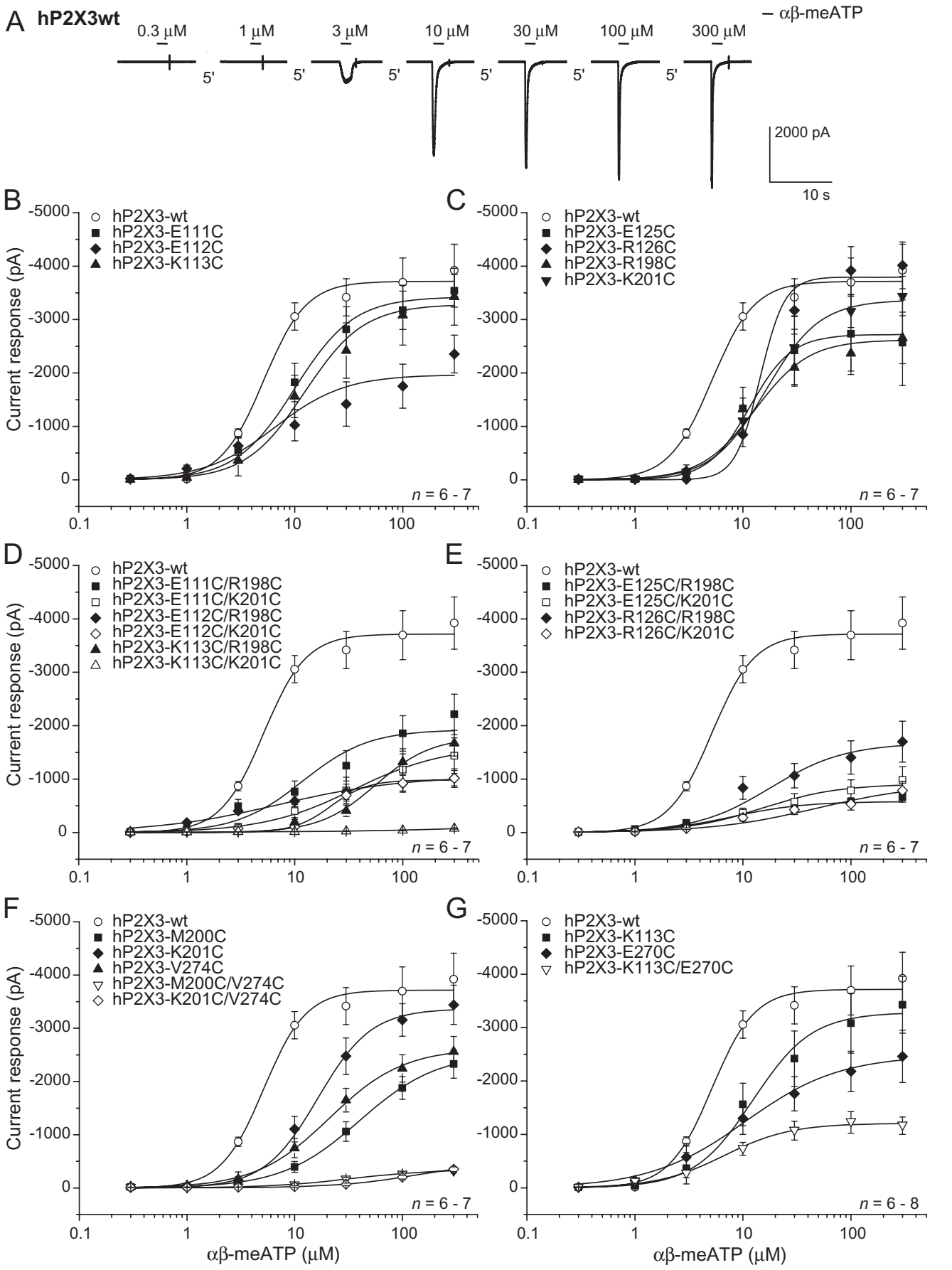
A hP2X3wt
0.3 μM
1 μM
3 μM
10 μM
30 μM
100 μM
300 μM
5'
– αβ-meATP
2000 pA
10 s
B
C
D
E
F
G
Current response (pA)
hP2X3-wt
hP2X3-E111C
hP2X3-E112C
hP2X3-K113C
hP2X3-E125C
hP2X3-R126C
hP2X3-R198C
hP2X3-K201C
hP2X3-E111C/R198C
hP2X3-E111C/K201C
hP2X3-E112C/R198C
hP2X3-E112C/K201C
hP2X3-K113C/R198C
hP2X3-K113C/K201C
hP2X3-E125C/R198C
hP2X3-E125C/K201C
hP2X3-R126C/R198C
hP2X3-R126C/K201C
hP2X3-M200C
hP2X3-K201C
hP2X3-V274C
hP2X3-M200C/V274C
hP2X3-K201C/V274C
hP2X3-K113C
hP2X3-E270C
hP2X3-K113C/E270C
n = 6 - 7
n = 6 - 8
αβ-meATP (μM)

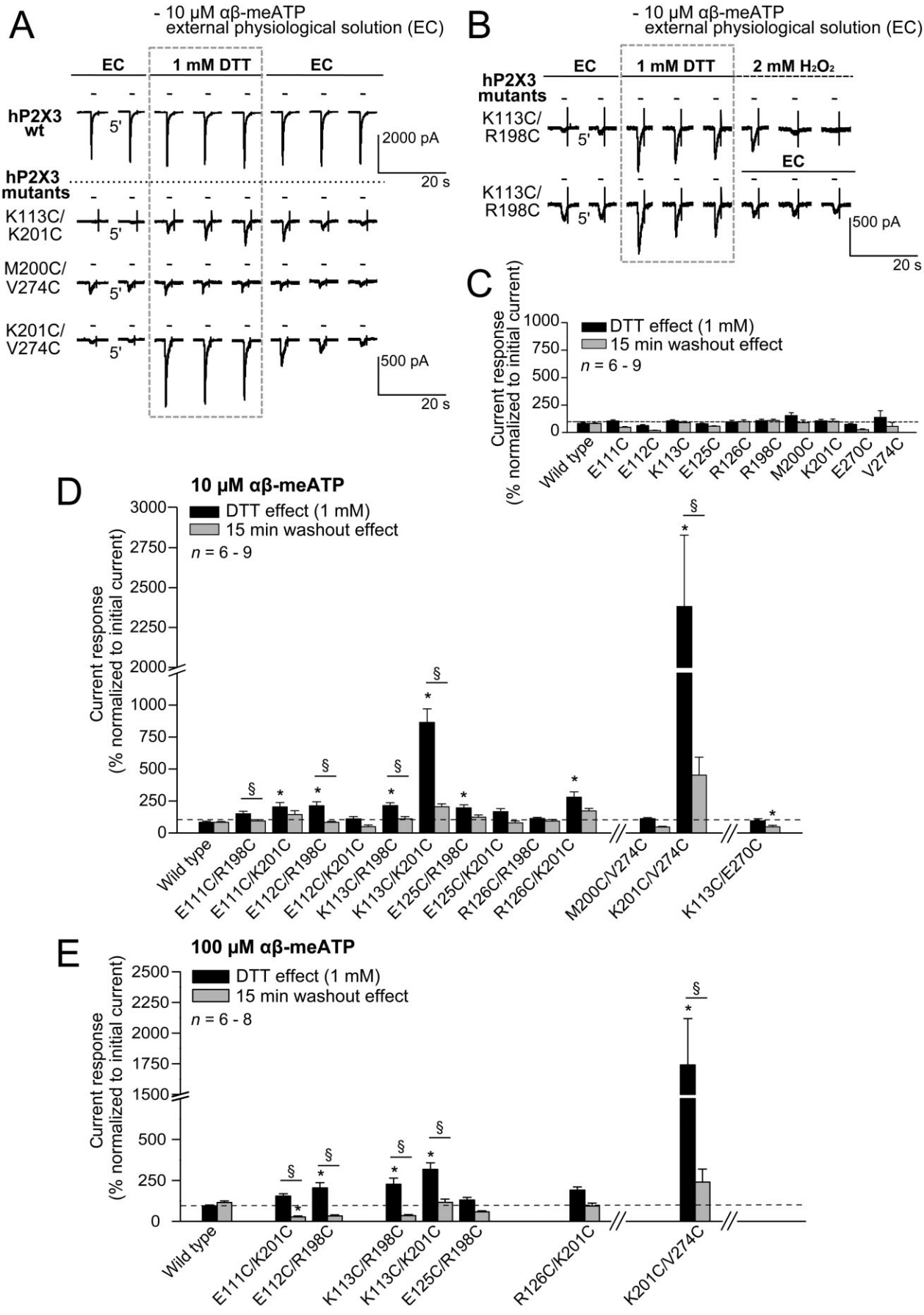
A
- 10 μM αβ-meATP
external physiological solution (EC)
EC
1 mM DTT
EC
hP2X3 wt
hP2X3 mutants
K113C/ K201C
M200C/ V274C
K201C/ V274C
5'
2000 pA
20 s
500 pA
20 s
B
- 10 μM αβ-meATP
external physiological solution (EC)
EC
1 mM DTT
2 mM H2O2
hP2X3 mutants
K113C/ R198C
EC
500 pA
20 s
C
Current response (% normalized to initial current)
DTT effect (1 mM)
15 min washout effect
n = 6 - 9
Wild type
E111C
E112C
K113C
E125C
R126C
R198C
M200C
K201C
E270C
V274C
D
10 μM αβ-meATP
DTT effect (1 mM)
15 min washout effect
n = 6 - 9
Current response (% normalized to initial current)
Wild type
E111C/R198C
E111C/K201C
E112C/R198C
E112C/K201C
K113C/R198C
K113C/K201C
E125C/R198C
E125C/K201C
R126C/R198C
R126C/K201C
M200C/V274C
K201C/V274C
K113C/E270C
E
100 μM αβ-meATP
DTT effect (1 mM)
15 min washout effect
n = 6 - 8
Current response (% normalized to initial current)
Wild type
E111C/K201C
E112C/R198C
K113C/R198C
K113C/K201C
E125C/R198C
R126C/K201C
K201C/V274C

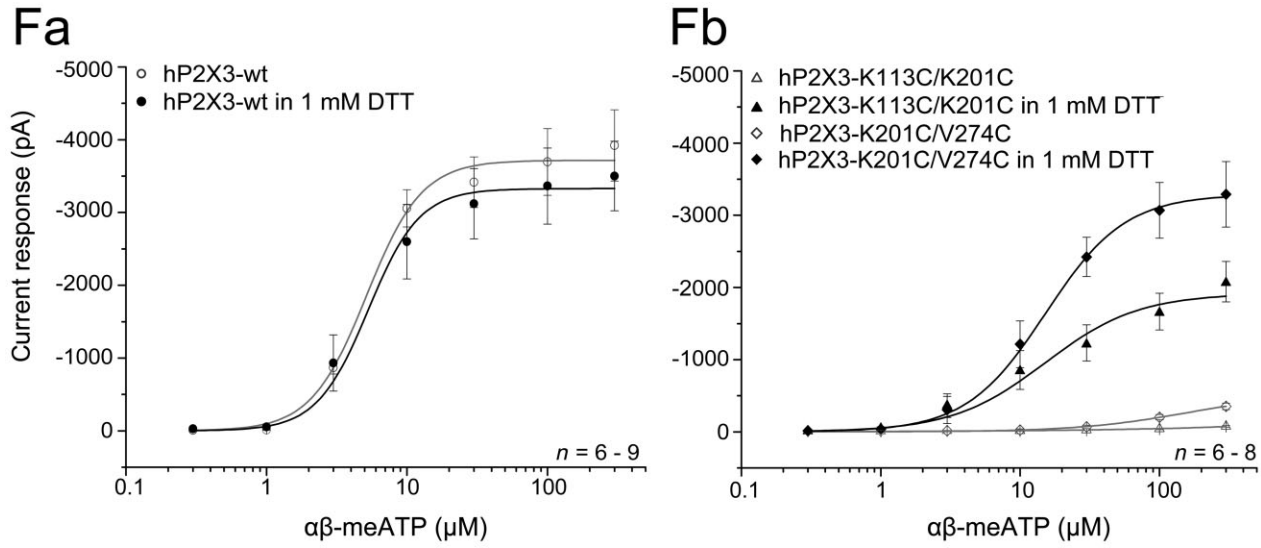

Figure 3

Reversibility of disulfide bond formation in the cysteine single and double mutant hP2X3 receptors expressed in HEK293 cells by DTT. Whole-cell patch clamp recordings were made as described in the legend for Figure 2. A test concentration of α,β-meATP (10 μM) was applied for 2 s every 5 min to HEK293 cells expressing wt hP2X3, as well as its cysteine single and double mutants. The effect of α,β-meATP was evaluated before, during and after superfusion with DTT (1 mM) in EC for 15 min. (A) The DTT-reversibility protocol is shown for wt hP2X3 and its selected cysteine double mutants. EC, external physiological solution. (B) DTT washout with EC alone or with 2 mM H_2O_2-containing EC showed no difference. Effect of DTT on HEK293 cells expressing wt hP2X3 or its cysteine single (C) and double mutants (D and E). (D) Double mutants were selected, at which DTT caused a statistically significant increase of the α,β-meATP (10 μM) currents. (E) Experiments were repeated by using a higher concentration (100 μM) of α,β-meATP. Currents after DTT treatment and a further washout period were normalized to initial currents (100%; dashed line). Each column indicates the mean ± SEM of 6–9 cells. *$P < 0.05$, significant difference from the pre-DTT current amplitude; §$P < 0.05$, significant difference between DTT and washout effect). (F, panels a, b) Concentration–response relationships of α,β-meATP at HEK293 cells transfected with the wt hP2X3 receptor (F, panel a) or its cysteine double mutants K113C/K201C or K201C/V274C (F, panel b). Increasing concentrations of α,β-meATP (0.3–300 μM) were applied locally for 2 s with 5 min intervals at a holding potential of –65 mV in the presence (black lines) or absence (grey lines) of 1 mM DTT. Each symbol indicates the mean ± SEM of 6–9 cells. The EC_{50}, I_{max} values and Hill coefficients n_H were as follows; wt P2X3, 5.3 ± 1.3 μM, –3328.7 ± 238.3 pA, 2.4 ± 0.4; K113C/K201C, 15.2 ± 4.8 μM, –1916.0 ± 181.8 pA, 1.3 ± 0.1; K201C/V274C, 15.3 ± 2.9 μM, –3289.0 ± 230.4 pA, 1.5 ± 0.1. In the presence of DTT, the EC_{50} values of both double mutants differed from those of the wt P2X3 receptor. However, DTT depressed only the I_{max} of K113C/K201C-hP2X3, when compared with the wt receptor (*$P < 0.05$; one-way ANOVA, each).

with the respective values measured in DTT-free conditions (Figure 3F, panel a; Table 1). By contrast, DTT partially rescued the strongly diminished effect of α,β-meATP at the two double mutants (Figure 3F, panel b; Table 1).

To decide whether the agonist α,β-meATP (and thus channel opening) is necessary for the reversibility of the DTT effect on the cysteine double mutants K113C/K201C and K201C/V274C, we slightly changed the standard experimental protocol (see the Methods section). Instead of applying α,β-meATP (10 μM) 5 min after washing out DTT, we superfused the HEK293 cells for another 5 min with DTT and applied α,β-meATP only after another 5 min (Supporting Information Fig. S3B). At both mutants, the agonist-induced currents decreased in a similar manner either with or without the co-application of α,β-meATP and DTT before finishing the incubation period (compare Figure 3A and Supporting Information Fig. S3B). Thus, disulfide bonds reinstated after washing out DTT, both immediately after finishing α,β-meATP application (with some residual binding of the agonist at the desensitized receptor, and subsequent gradual recovery) and 5 min after the end of α,β-meATP application (no residual agonist at the receptor and complete recovery). Thus, the (re)formation of disulfide bonds occurs also in the absence of an agonist and did not require an agonist-induced binding jaw movement.

It has recently been described that tightening of the ATP binding jaw of rat (r)P2X2 receptors by the introduction of extracellular histidines, and subsequently bridging them with Zn^{2+}, caused spontaneous channel openings (Jiang *et al.*, 2012). We did not observe spontaneous current responses at any of the cysteine double mutants before or after α,β-meATP application during the 15 s recording periods (see, e.g. Figure 2A). However, a systematic search for such currents, possibly induced by disulfide cross-linking of adjacent subunits, was not carried out in this study.

Molecular dynamics simulation of the ectodomain movement of the hP2X3 reveals the basis for the generation of disulfide bonds between a few identified double mutants

To interpret the ectodomain movement in the hP2X3 receptor, the distance between the backbones of each AA of a double mutant investigated was measured over the whole

Table 1

Concentration–response curve properties of the wt hP2X3 receptor and its cysteine single and double mutants

Mutants	EC_{50} (μM)	I_{max} (pA)	n_H	n
I				
Wild type (wt)	5.2 ± 0.5	−3718.5 ± 99.8	2.2 ± 0.3	7
II				
E111C	10.0 ± 1.8[a,*]	−3423.5 ± 175.6	1.6 ± 0.1	6
E112C	6.6 ± 2.7	−1968.7 ± 285.2	1.3 ± 0.2	7
K113C	12.4 ± 2.1[a,*]	−3281.8 ± 209.3	1.6 ± 0.1	6
E125C	11.6 ± 5.6	−2722.1 ± 757.2	2.3 ± 0.4	7
R126C	14.4 ± 5.4	−3796.3 ± 783.4	3.8 ± 1.0	6
R198C	12.9 ± 5.8	−2620.5 ± 602.4	1.8 ± 0.3	7
M200C	40.1 ± 1.3[a,*]	−2526.9 ± 30.5	1.2 ± 0.1	6
K201C	16.4 ± 4.0[a,*]	−3367.5 ± 305.6	1.8 ± 0.2	6
E270C	10.48 ± 1.7[a,*]	−2479.0 ± 108.7[a,*]	1.0 ± 0.1	8
V274C	21.1 ± 3.6[a,*]	−2624.1 ± 159.1[a,*]	1.3 ± 0.1	6
III				
E111C/R198C	11.9 ± 4.8	−1925.9 ± 313.4[a,*]	1.4 ± 0.1	7
E111C/K201C	35.3 ± 12.6[a,*]	−1612.6 ± 230.1[a,b,c,*]	1.0 ± 0.1	7
E112C/R198C	7.3 ± 1.9	−1053.3 ± 65.9[a,c,*]	0.8 ± 0.1	6
E112C/K201C	21.6 ± 1.9[a,*]	−984.3 ± 34.9[a,b,c,*]	2.5 ± 0.4	6
K113C/R198C	56.3 ± 6.9[a,*]	−1788.3 ± 101.2[a,*]	1.7 ± 0.2	6
K113C/K201C	nc	nc	nc	6
E125C/R198C	15.8 ± 3.4[a,*]	−722.2 ± 40.6[a,*]	1.3 ± 0.2	6
E125C/K201C	15.0 ± 3.5[a,*]	−909.2 ± 100.9[a,b,c,*]	1.2 ± 0.1	6
R126C/R198C	18.0 ± .8.5	−1675.3 ± 315.9[a,*]	1.3 ± 0.2	7
R126C/K201C	48.5 ± 51.1	−911.6 ± 391.5[a,b,c,*]	0.9 ± 0.1	7
IV				
M200C/V274C	32.7 ± 5.7[a,*]	−348.4 ± 21.4[a,b,c,*]	1.1 ± 0.2	6
K201C/V274C	156.5 ± 54.2[a,*]	−527.4 ± 86.7[a,b,c,*]	1.1 ± 0.2	7
V				
K113C/E270C	6.7 ± 1.4	−1208.0 ± 95.1[a,b,c,*]	1.4 ± 0.1	8

Half maximal effective concentration (EC_{50}), maximal current response (I_{max}) and Hill coefficient (n_H) as well as the number of measured HEK293 cells expressing the mutant or wt hP2X3 receptor (*n*). Values represent mean ± SEM.
*$P < 0.05$ (one-way ANOVA).
[a]EC_{50} and I_{max} values are significantly different from those measured in wt P2X3.
[b]The I_{max} value of the double mutant is significantly different from that of the first corresponding single mutant.
[c]The I_{max} value of the double mutant is significantly different from that of the second corresponding single mutant.
nc, non-calculable; I, wild type; II, cysteine single mutants; III, cysteine double mutants cross-linking beak and dorsal fin; IV, cysteine double mutants cross-linking dorsal fin and left flipper; V, cysteine double mutants cross-linking beak and left flipper.

simulation period of 243 ns (Figure 4). Only those double mutants that exhibited a robust potentiation of their current responses by DTT on the application of both 10 and 100 μM α,β-meATP (E112C/R198C, K113C/R198C, K113C/K201C; Figure 4A and B) and K201C/V274C (Figure 4C and D) were taken into consideration. In the three first-mentioned cysteine double mutants, head and dorsal fin of adjacent receptor subunits approach each other transiently after 20 ns, then shortly diverge, and subsequently converge again after about 90 ns (E111C/K201C behaved in a similar manner, but is not shown in the Figure 4A for better visibility). By contrast, in the K201C/V274C-hP2X3 receptor, neighbouring regions of the left flipper and dorsal fin are in close approximation over the entire simulation period (Figure 4C).

Further, the obtained distances between paired AAs at neighbouring regions were plotted in histograms and data were fitted by two Gaussian curves illustrating closeness and distance of one pair of mutants (Figure 4B and D). For the mutants E112C/R198C, K113C/R198C and K113C/K201C, the histograms showed two rather clearly separated peaks characterizing two steady states (Figure 4B). Because the first peak is narrower than the second one, we conclude that

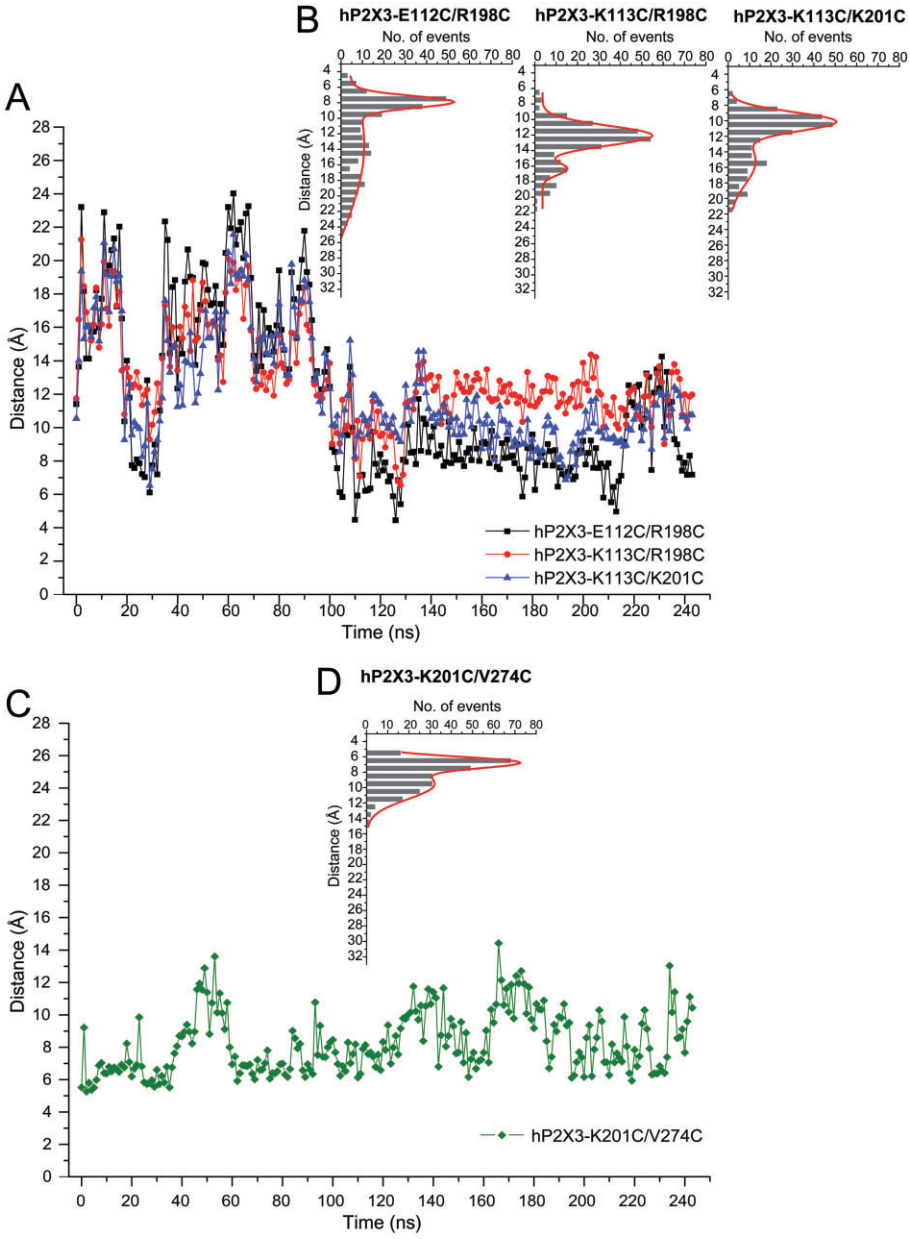

Figure 4

Analysis of the distance between backbones of pairs of the corresponding cysteine double mutants of the hP2X3 receptor at neighbouring receptor subunits during the first 243 ns of molecular dynamics simulation. Beak-dorsal fin contacts: E112C/R198C, K113C/R198C, K113C/K201C (A); dorsal fin-left flipper contacts: K201C/V274C (C). (B, D) Histograms of the distance (in angstrom) against the number of events of selected double mutants from panel (A) and (C) (grey bars). Data were fitted by two Gaussian curves and the peaks might be interpreted as two states (red line).

chances for a convergence of two opposing AAs are larger during the first than during the second peak. In contrast, with the cysteine double mutant K201C/V274C, the two peaks partially merged together (Figure 4D), which of course markedly increased the chances of AA convergence during the whole observation period. It remains to be explained why the calculated distances between the AA pairs were in our simulation somewhat larger than ~4.6 Å needed for the generation of S–S bonds. There are three possible reasons for this discrepancy: (i) the time resolution of our simulation is not high enough to reliably follow very short approaches of the relevant AAs; (ii) the follow-up period of 243 ns is not long enough to notice S–S bond formation occurring later on; and (iii) the distances between the relevant AAs are measured at the backbone but not between their side chains, which may acquire variable positions.

Cell surface trafficking of hP2X3 receptor cysteine double mutants and inter-subunit disulfide cross-linking in HEK293 cells

We performed biochemical analysis of the His-tagged hP2X3 subunit and the corresponding cysteine double mutants

stably expressed in HEK293 cells to demonstrate the plasma membrane expression and the homotrimeric assembly of all mutants, even those with impaired function. Furthermore, we have analysed the disulfide-mediated cross-linking of neighbouring subunits in the inter-subunit cysteine double mutants by this biochemical approach.

Amino-reactive labelling of the His-hP2X3 receptor and its mutants by a membrane-impermeant fluorescent dye (see the Methods section) enabled us to selectively visualize the plasma membrane-inserted fraction of the hP2X3 proteins. SDS-PAGE analysis of the wt and the indicated cysteine double mutants of the hP2X3 receptor revealed that all mutants were transported to the cell surface (Figure 5A). Also, functionally impaired hP2X3 mutants were capable of being expressed at the cell surface. The selected inter-subunit cysteine double mutants appeared under non-reducing conditions as SDS-resistant oligomeric complexes at the plasma membrane (Figure 5A, lanes with odd numbers) in contrast to the wt hP2X3 subunit, which did not form disulfide adducts (Figure 5A, panel a, lane 1). As expected, chemical reduction by DTT was able to break the oligomeric complex to the monomer level (Figure 5A, lanes with even numbers), indicating that the formation of the SDS-resistant oligomeric complexes is due to disulfide-mediated cysteine cross-linking of the neighbouring inter-subunit cysteine residues. In case of the E111C/R198C-hP2X3 and E111C/K201C-hP2X3, the existence of significant amounts of monomeric and dimeric forms in the absence of DTT (lanes 3 and 5) indicates a lower level of spontaneous cross-linking as compared to the almost complete cross-linking of the other double mutants.

BN-PAGE analysis revealed that all the analysed hP2X3 cysteine double mutants were capable of correctly assembling to homotrimers that appeared at the cell surface in the same manner as the wt hP2X3 receptor (Figure 5B, panel a, lanes 1 and 4–11; Figure 5B, panel b, lanes 1 and 4–8). While the wt hP2X3 receptor dissociated into dimers and monomers by partial denaturing with 0.1% SDS (Figure 5B, panels a and b, lane 2), the homotrimeric form of the cysteine double mutants resisted to dissociate into lower order intermediates when treated with 0.1% SDS alone (Figure 5B, panel a, lane 12). However, dissociation was achieved by the combined treatment with SDS and DTT (Figure 5B, panel a, lane 13; the example shown is for K201C/V274C). These findings clearly indicate that in contrast to the wt receptor, the hP2X3 cysteine double mutants are quantitatively cross-linked at the homotrimeric level by disulfide bonds formed between the introduced inter-subunit cysteine residues. A notable exemption is the homotrimeric K113C/E270C double mutant, which required only SDS to dissociate into its monomers. This observation is consistent with the prediction from our homology model that the K113C/E270C double mutation leads to the formation of an intra-subunit disulfide bridge rather than to inter-subunit cross-linking.

Cell surface trafficking of hP2X3 receptor mutants and disulfide cross-linking in X. laevis *oocytes*

To check for expression system-specific differences, we performed similar biochemical experiments in the non-mammalian *X. laevis* oocyte expression system. We again addressed the question whether the cysteine single or double mutants of the homotrimeric hP2X3 receptor, of which some showed an impaired function, were able to correctly assemble and to be expressed at the plasma membrane in *X. laevis* oocytes. Furthermore, we also demonstrated the disulfide-mediated cross-linking of neighbouring subunits in inter-subunit cysteine double mutants by biochemical approaches. Firstly, to verify that the functional data obtained in HEK293 cells and *X. laevis* oocytes are basically identical, we functionally tested the wt and some selected inter-subunit cysteine double mutants of the hP2X3 receptor by TEVC after expression in oocytes. In fact, in oocytes injected with cRNAs for the wt hP2X3 receptor or the double mutants E112C/R198C, K113C/K201C, M200C/V274C and K201C/V274C, we observed similar functional evidence for disulfide bond formation as in HEK293 cells. As shown in Supporting Information Fig. S4A and B, the α,β-meATP (10 μM)-induced current amplitudes of the selected inter-subunit cysteine double mutants were modulated virtually in the same manner by the reducing reagent DTT in oocytes as in HEK293 cells (cf. Figure 3A and D).

SDS-PAGE analysis of the indicated cysteine single or double mutants of the hP2X3 receptor revealed that all mutants were transported to the cell surface as efficiently as the wt hP2X3 receptor; this was revealed by selective visualization of the plasma membrane-inserted fraction of the hP2X3 proteins (Supporting Information Fig. S4C and D). Functionally impaired hP2X3 mutants were also capable of appearing at the cell surface. These experiments show in addition that the selected inter-subunit cysteine double mutants appeared under non-reducing conditions as SDS resistant oligomeric complexes at the plasma membrane (Supporting Information Fig. S4C, panels b and c, lanes with odd numbers). By comparison, the single cysteine mutants and the K113C/E270C-hP2X3 mutant forming a putative intra-subunit disulfide bond migrated exclusively as monomers in the absence and presence of DTT in the SDS-PAGE (Supporting Information Fig. S4C, panel c), which indicates the absence of unspecific cross-linking of introduced cysteines with the native cysteines of the hP2X3 subunit. As expected, in cysteine double mutants, chemical reduction by DTT was able to break the oligomeric complex to the monomer level (Supporting Information Fig. S4C, panels b, c, lanes with even numbers), indicating that the formation of the SDS-resistant oligomeric complexes is due to disulfide-mediated cysteine cross-linking of the neighbouring inter-subunit cysteine residues. Interestingly, also mutants that showed only a minimally increased current amplitude after DTT treatment, such as the M200C/V274C-hP2X3 mutant, were as efficiently cross-linked as the K201C/V274C-hP2X3 mutant, which exhibited a maximal increase of the current amplitude by DTT.

BN-PAGE analysis revealed that all the analysed hP2X3 cysteine mutants were capable of correctly assembling to homotrimers that appeared at the cell surface in the same manner as the wt hP2X3 receptor (Supporting Information Fig. S4D, panel a, lanes 1 and 4–10; Supporting Information Fig. S4D, panel b, lanes 1 and 4–11; Supporting Information Fig. S4D, panel c, lanes 1, 4–10 and 13). While the wt hP2X3 receptor, the cysteine single mutants and the K113C/E270C-hP2X3 mutant dissociated into dimers and monomers by partial denaturing with 0.1% SDS (Supporting Information

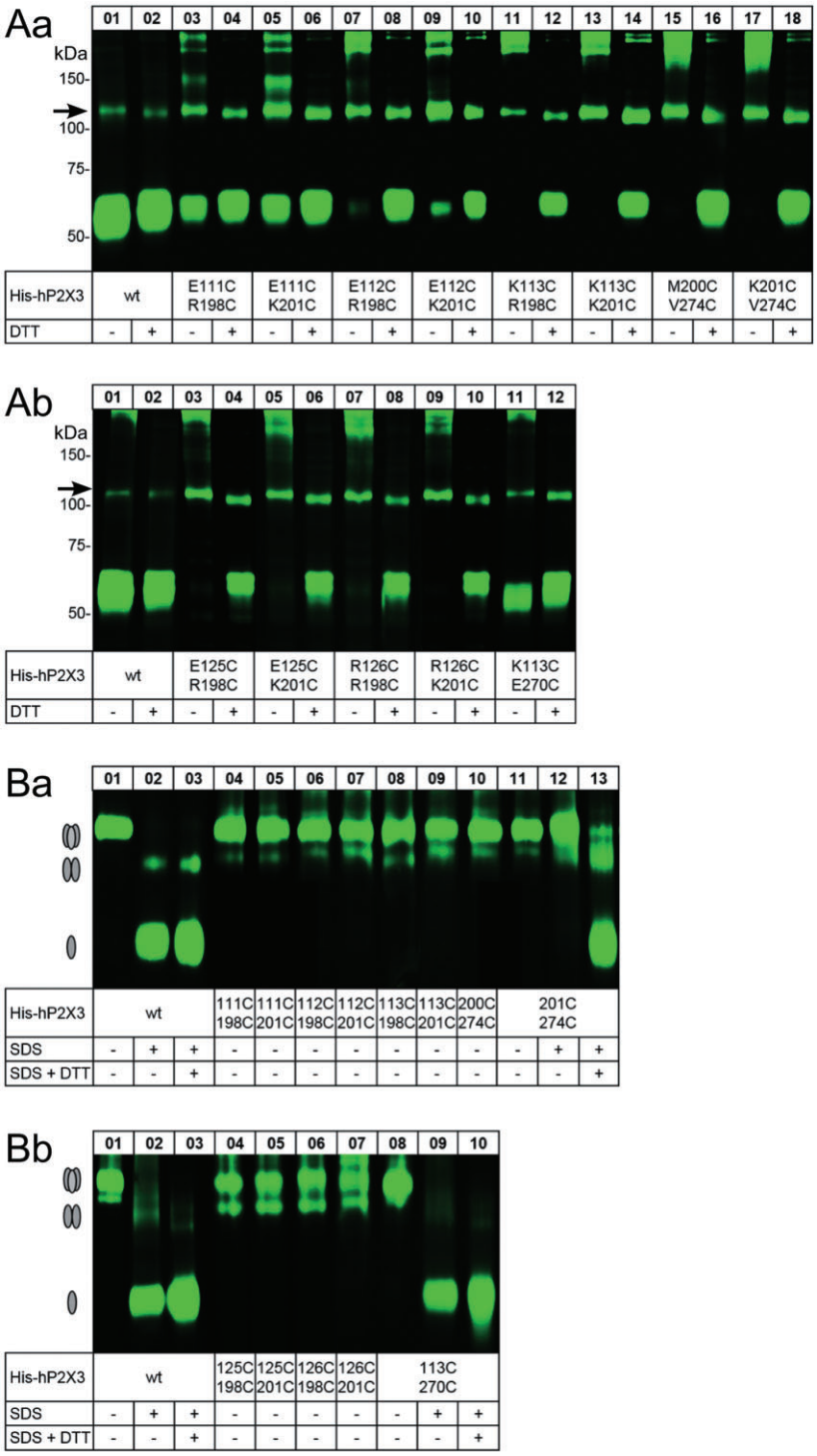

Figure 5

Plasma membrane expression and assembly of the hP2X3 receptor and its mutants in Tet-on HEK293 cells. (A, panels a, b) The plasma membrane-bound form of the indicated hP2X3 variants was covalently labelled with IR800, purified by Ni-NTA chromatography, resolved by non-reducing and reducing SDS-PAGE and visualized by fluorescence scanning. The arrow indicates the migration position of a non-specific background band that was present in variable intensities in this and some other experiments. (B, panels a, b) The indicated plasma membrane-bound hP2X3 proteins were resolved by BN-PAGE in the non-denatured state and exemplarily after partial denaturation following a 1 h incubation with SDS and/or DTT at 37°C. Note that the homotrimeric form of the wt hP2X3 dissociated in 0.1% SDS into dimers and mostly monomers, while the homotrimeric form of the cysteine double mutant required reduction of disulfide bonds by DTT in addition to SDS to dissociate, as shown exemplarily for the K201C/V274C mutant. The ovals in the left margins indicate the numbers of hP2X3 subunits incorporated in the respective protein band.

Fig. S4D, panel a, lanes 2 and 11, panel b, lane 2 and panel c, lanes 2 and 14), the homotrimeric form of the cysteine double mutants resisted to dissociate into lower order intermediates when treated with 0.1% SDS alone, as shown for the K201C/V274C-hP2X3 (Supporting Information Fig. S4D, panel b, lane 12) or the R126C/K201C mutant (Supporting Information Fig. S4D, panel c, lane 11). However, ready dissociation was achieved by the combined treatment with SDS and DTT (Supporting Information Fig. S4D, panel b, lane 13; Supporting Information Fig. S4D, panel c, lane 12). These findings clearly indicate that in contrast to the wt and cysteine single mutants, the cysteine double mutants are quantitatively cross-linked at the homotrimeric level by disulfide bonds formed between the introduced inter-subunit cysteine residues.

Taken together, the functional data obtained from HEK293 cells were consistent with our functional and biochemical findings in *X. laevis* oocytes. All the mutants analysed were capable of homotrimeric assembly and plasma membrane expression. Furthermore, the cysteine double mutants were quantitatively cross-linked by inter-subunit disulfide bonds to homotrimers.

Visualization of ATP binding to wt P2X3 and mutants at the surface of X. laevis *oocytes*

To address the question whether the disulfide bonds found to block the α,β-meATP-induced opening of the hP2X3 channel pore did so by interfering with agonist binding or with channel gating, we performed binding experiments with a fluorescent analogue of ATP, BODIPY ATP. To this end, we first characterized BODIPY ATP functionally. In both wt hP2X3 receptor-expressing HEK293 cells and wt hP2X3-expressing *X. laevis* oocytes, BODIPY ATP elicited inward currents with similar concentration dependencies (Figure 6A and B). In the HEK293 cells, each concentration of BODIPY ATP was applied three times with first a 2 s and then a second 60 s interval as indicated, followed by a 5 min washout and recovery period, before the next higher concentration of BODIPY ATP was applied. This protocol enabled us to deduce EC_{50} values and binding energies (ΔG) of BODIPY ATP for the hP2X3 receptor without recording complete concentration–response curves (the high costs of BODIPY ATP were an apparent obstacle) by applying a hidden Markov model, which describes the channel behaviour during agonist binding (Riedel *et al.*, 2012). With an EC_{50} value of 3.6 ± 0.1 μM and a ΔG of –30.5 kJ·mol^{-1}, BODIPY ATP possesses a similar potency as genuine ATP at the hP2X3 receptor (experimental and simulated EC_{50} values of 2.5 ± 1.8 and 3.0 ± 0.1 μM ATP, respectively, see Riedel *et al.*, 2012). The unchanged ability of BODIPY ATP in activating the hP2X3 receptor can be explained by the linkage of the fluorophore to the ribose moiety of ATP, which apparently does not interfere with the binding to the ATP binding pocket. This notion is further underscored by the equipotent activation of the wt P2X3 receptor in *X. laevis* oocytes by BODIPY ATP and α,β-meATP (Figure 6B).

The current responses of the wt hP2X3 receptor to 0.1 μM BODIPY ATP were small, but well detectable and were not increased following DTT treatment (Figure 6C). The current response of the K201C/V274C-hP2X3 mutant to 0.1 μM BODIPY ATP was almost undetectable, but strongly increased following DTT treatment (Figure 6C). Thus, the data obtained with ATP in HEK293 cells (Figure 3A) could be fully reproduced with BODIPY ATP in *X. laevis* oocytes. This finding was an important prerequisite for the following binding experiments.

Next, we attempted to assess the binding of BODIPY ATP to the plasma membrane-expressed P2X3 receptor. HEK293 cells turned out to be unsuited for this purpose because they strongly bound BODIPY ATP in a non-specific manner in the absence of hP2X3 receptor expression (data not shown). Unlike HEK293 cells, *X. laevis* oocytes showed virtually no non-specific binding of BODIPY ATP when analysed over time by a confocal laser scanning microscope (Figure 6D, upper panel). In oocytes expressing the wt hP2X3 receptor, incubation with BODIPY ATP resulted in a time-dependent fluorescence labelling of the plasma membrane (Figure 6D, middle panel). In contrast, the plasma membrane of oocytes expressing the K201C/V274C double mutant was barely stained by BODIPY ATP under non-reducing conditions. However, following incubation with DTT, the plasma membrane became strongly labelled apparently because the breaking of the disulfide bonds enabled BODIPY ATP to dock into the ATP binding site. This finding is not only in complete agreement with the functional data (Figure 6C), but also provides strong evidence that the K201C/V274C disulfide bond acts in the first instance by preventing agonist binding. We cannot exclude that the gating is also affected by the

Figure 6

Visualization of agonist binding using BODIPY ATP. Shown are characteristic fast desensitizing P2X3 current responses to BODIPY ATP in HEK293 cells (A) and *X. laevis* oocytes (B and C). (A) Averaged current responses of three HEK293 cells, transfected with wt hP2X3, to BODIPY ATP. BODIPY ATP was applied for 2 s (horizontal bars) in 2 and 60 s intervals; 5′ indicates the 5 min recovery interval between the application of increasing BODIPY ATP concentrations. (B) Current responses of *X. laevis* oocytes, expressing wt hP2X3, were elicited by increasing concentrations of BODIPY ATP or α,β-meATP, applied for 10 s every 5 min (horizontal bars). (C) BODIPY ATP was applied to *X. laevis* oocytes (horizontal bars) expressing the wt hP2X3 or the hP2X3-K201C/V274C mutant (left and right set of two current traces each respectively). DTT (1 mM) was present for 5 min before and during BODIPY ATP application to the hP2X3-K201C/V274C receptor mutant as indicated. (D) Confocal laser scanning microscopic visualization of BODIPY ATP binding to the surface of intact *X. laevis* oocytes not expressing or expressing the wt P2X3 receptor or its mutant at the indicated time points: at 0 s, directly after 0.1 μM BODIPY ATP application; at 9 min, immediately before 1 mM DTT application; at 24 min, when finishing recording. Please note that BODIPY ATP did not bind to control (non-injected) oocytes. (E) The relative fluorescence intensity (in arbitrary units) of the plasma membrane was assessed in 1 min intervals by normalizing the difference of the fluorescence intensities of ROI1 and ROI2 (background fluorescence). (F) The encircled areas illustrate the two typical regions of interest, ROI1 and ROI2, used for the calculation of the plasma membrane-bound fluorescence intensity. (G) Time course of the binding of BODIPY ATP to wt hP2X3 expressing oocytes in the absence of DTT. (H) Time course of the displacement of bound BODIPY ATP by α,β-meATP. Data in (E), (G) and (H) are means ± SEM from 7 to 10 oocytes per time point.

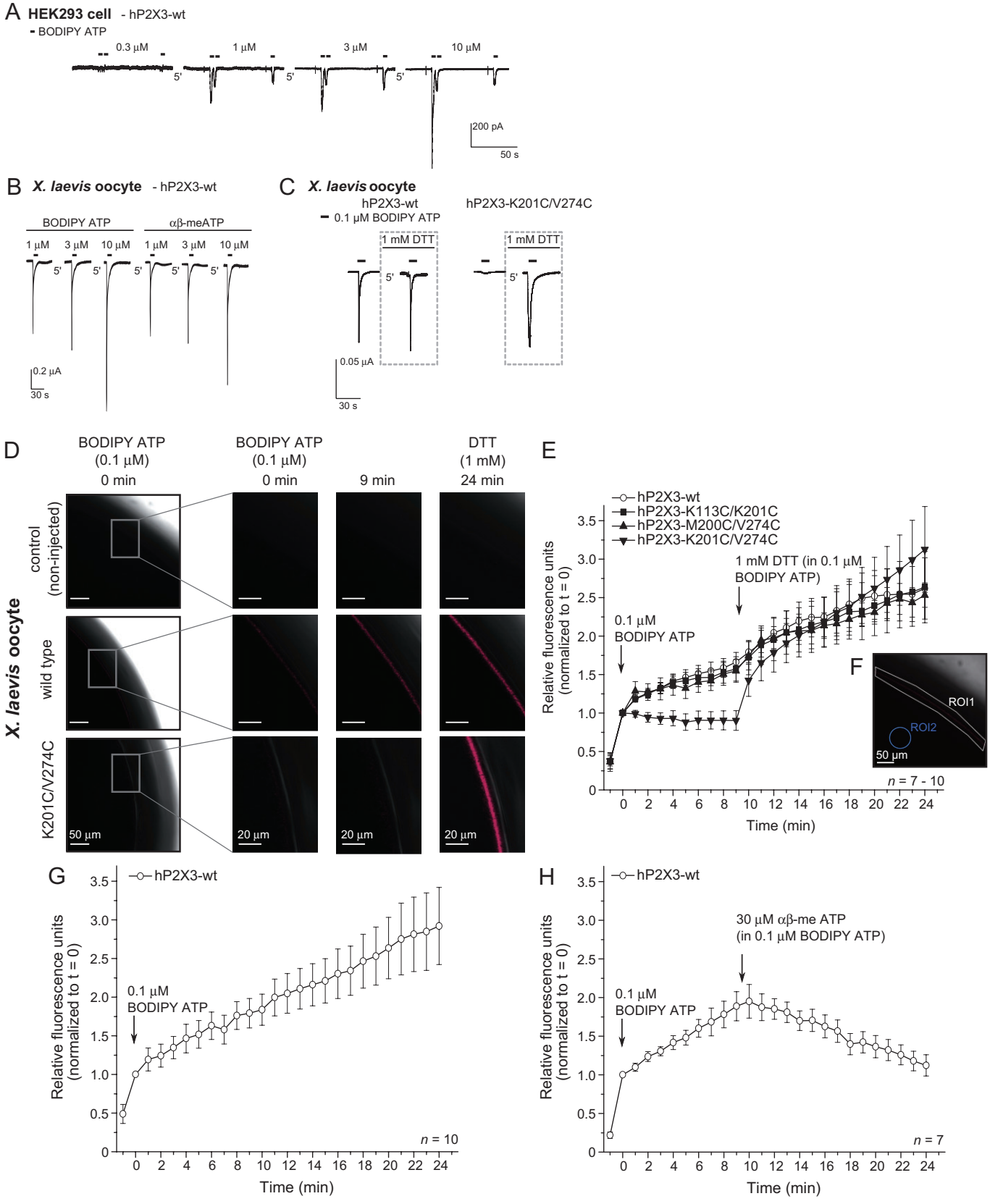
A HEK293 cell - hP2X3-wt
- BODIPY ATP
0.3 μM
1 μM
3 μM
10 μM
5'
200 pA
50 s
B X. laevis oocyte - hP2X3-wt
BODIPY ATP
αβ-meATP
1 μM
3 μM
10 μM
0.2 μA
30 s
C X. laevis oocyte
hP2X3-wt
hP2X3-K201C/V274C
- 0.1 μM BODIPY ATP
1 mM DTT
0.05 μA
30 s
D
X. laevis oocyte
BODIPY ATP (0.1 μM) 0 min
BODIPY ATP (0.1 μM) 0 min
9 min
DTT (1 mM) 24 min
control (non-injected)
wild type
K201C/V274C
50 μm
20 μm
E
hP2X3-wt
hP2X3-K113C/K201C
hP2X3-M200C/V274C
hP2X3-K201C/V274C
1 mM DTT (in 0.1 μM BODIPY ATP)
0.1 μM BODIPY ATP
Relative fluorescence units (normalized to t = 0)
Time (min)
n = 7 - 10
F
ROI1
ROI2
50 μm
G
hP2X3-wt
0.1 μM BODIPY ATP
Relative fluorescence units (normalized to t = 0)
Time (min)
n = 10
H
hP2X3-wt
30 μM αβ-me ATP (in 0.1 μM BODIPY ATP)
0.1 μM BODIPY ATP
Relative fluorescence units (normalized to t = 0)
Time (min)
n = 7

K201C/V274C disulfide bond, but this is certainly secondary to the prevention of binding.

To exclude the possible effect of 1 mM DTT on the background fluorescence of 0.1 μM BODIPY ATP, we performed measurements with oocytes incubated with ORi supplemented or not with 1 mM DTT (Supporting Information Fig. S5A). Confocal laser scanning microscopy failed to demonstrate any fluorescence change by DTT. In addition, a fluorescence spectrometer was used to determine the possible change in the fluorescence of BODIPY ATP (1 μM) by DTT (1 mM) (Supporting Information Fig. S5B). An emission spectrum from 600 to 650 nm was determined with an excitation maximum at 592 nm. There was no difference between the fluorescence intensities of BODIPY ATP alone or together with DTT, and DTT alone did not cause any fluorescence.

To quantify the relative changes of the plasma membrane-bound fluorescence, two regions of interest were selected as exemplified in the inset of Figure 6E (Figure 6F). A low background fluorescence was noted immediately after the application of BODIPY ATP at 0 min (Figure 6E–H), which is most likely due to the presence of BODIPY ATP in the solution, as noted previously with Alexa-647 ATP (Bhargava *et al.*, 2013). The plasma membrane-bound fluorescence intensity increased steadily with time (Figure 6E–H). The bound BODIPY ATP fluorescence could be competitively displaced by α,ß-meATP, underscoring the specificity of the binding (Figure 6H).

BODIPY ATP was bound to the cysteine double mutant K113C/K201C and M200C/V274C with a virtually identical rate as to the wt P2X3 receptor (Figure 6E). DTT applied 9 min after starting the application of BODIPY ATP had little, if any, effect on the binding of BODIPY ATP. This suggests that the ATP binding pocket of the K113C/K201C and M200C/V274C mutants is as readily accessible as that of the wt P2X3 receptor. In contrast, the K201C/V274C double mutant was unable to bind BODIPY ATP, as inferred from the unchanged fluorescence during the first 9 min of incubation with BODIPY ATP (Figure 6E). Breaking the disulfide bond by addition of DTT almost instantaneously enabled the binding of BODIPY ATP, indicating that the disulfide bond between residues 201 and 274 prevented the access of BODIPY ATP to the ATP binding pocket. In summary, we conclude that the engineering of disulfide bonds interfered with agonist binding in the cross-linked state of the K201C/V274C-hP2X3 mutant, but failed to have a similar effect in the K113C/K201C-hP2X3 and M200C/V274C-hP2X3 mutants, at least at the low concentration of BODIPY ATP used in our experiments.

The interpretation of the BODIPY ATP experiments is dependent upon the assumption that the local environment has no effect on the fluorescence. In fact, ligand-induced conformational changes of proteins may change the local environment and thus the fluorescence of fluorophores. However, it was shown in voltage-clamp fluorometry measurements on rP2X1 receptors expressed in *X. laevis* oocytes that fluorescence changes caused by conformational modifications of the receptor structure occur in the range of a few percent (depending upon the membrane area under study) (Lörinczi *et al.*, 2012) but never reach two- to three-fold changes of the fluorescence as found in the present study.

Discussion

In the present experiments, molecular dynamics simulation of movements in the hP2X3 receptor structure suggests the high flexibility of the ectodomain region of adjacent subunits relative to each other. These findings correlate with the finding that the ATP binding pouch is located at the interface of two neighbouring subunits formed by two nucleotide binding segments, NBS1–2 of one subunit and NBS3–4 of the adjacent subunit (Mager *et al.*, 2004; Bodnar *et al.*, 2011). The occupation of two of the three possible P2X binding pouches by ATP is sufficient to induce pore opening (Riedel *et al.*, 2007; Károly *et al.*, 2008; Hausmann *et al.*, 2012).

Based upon these simulations, we have selected pairs of AA residues possibly forming hydrogen bonds and salt bridges between adjacent receptor subunits and thereby participating in channel opening and closure (Jiang *et al.*, 2010; Khakh and North, 2012; Hausmann *et al.*, 2013). Residues E111, E112 and K113 (hP2X3 receptor numbering throughout) are located within the cysteine-rich head domain of P2X1, which has been shown by voltage-clamp fluorometry to undergo substantial movements during receptor opening and desensitization (Lörinczi *et al.*, 2012). Moreover, replacement of Ser-275 by Ala, Cys or Val changed the rate of desensitization and rate of recovery from desensitization after agonist application at hP2X3 receptors (Petrenko *et al.*, 2011). We generated a disulfide bond between M200 or K201 and V274, the AA located immediately adjacent to S275. In agreement with Petrenko *et al.* (2011), it was found that this region of the left flipper is highly important for receptor function. The role of the residual AAs chosen by us was, according to our knowledge, not hitherto investigated for receptor mobility.

In the following experiments, we tested inter-subunit and intra-subunit cysteine double mutants for their supposed ability to form disulfide bonds and thereby block α,β-meATP-induced currents. By formation of a disulfide bond, the receptor probably becomes immobilized in one state of operation, resulting in a loss of functionality. The reversibility of the disulfide bond formation caused by the reducing reagent DTT was associated with a recovery of receptor function. Chemical locks have been introduced in P2X receptors at the agonist binding site itself (Marquez-Klaka *et al.*, 2007; 2009; Agboh *et al.*, 2009; Jiang *et al.*, 2011; 2012; Roberts *et al.*, 2012), or in some cases, also at the lips of the binding jaw (Nagaya *et al.*, 2005) and found to inhibit agonist action (see also the Introduction section). Modifications of AAs directly involved in agonist binding should, of course, interfere with receptor activation. Although this is not the case when mutations are introduced in the lips of the binding jaw, disturbances in the subunit assembly and/or trafficking behaviour of the respective mutant receptors and their insertion into the plasma membrane still may occur.

Cysteine single mutants in the P2X1 (Roberts *et al.*, 2009; Allsopp *et al.*, 2011), P2X2 (Jiang *et al.*, 2000) and P2X4 (Roberts *et al.*, 2008) receptors were often utilized to identify AAs relevant for agonist binding. In contrast, the hP2X3 cysteine single mutants selected by us exhibited only slightly decreased agonist sensitivity compared with that of their wt counterpart, and DTT failed to restore the original situation. However, the inter-subunit cysteine mutations K113C/

K201C, M200C/V274C and K201C/V274C strongly depressed the α,β-meATP-induced currents. The reducing reagent DTT rescued the agonist effect only at the K113C/K201C and K201C/V274C mutants by breaking up disulfide bonds; molecular simulation suggested that the disulfide bond formed by M200C/V274C may be buried in the receptor structure, making it unaccessible for DTT.

A prerequisite for evaluating DTT effects at cysteine double mutants of hP2X3 was that α,β-meATP currents at the wt hP2X3 receptor should not be altered, in spite of the presence of 10 conserved cysteine residues in the extracellular loop forming five disulfide bonds (Clyne *et al.*, 2002; Ennion and Evans, 2002; Rokic *et al.*, 2010). It is assumed that the native disulfide bonds are either positioned in a hardly DTT accessible location or are indeed reduced, but without any effect for receptor function (Marquez-Klaka *et al.*, 2007; Roberts *et al.*, 2012).

Lörinczi *et al.* (2012) described for the P2X1 receptor the importance of movements in the cysteine-rich head domain (upper lip of the binding jaw) for receptor opening and desensitization. In fact, it has recently been suggested that the ATP-induced closure between the head and the dorsal fin leads finally to a rearrangement of the transmembrane helices of the P2X receptor in an iris-like movement (Hattori and Gouaux, 2012; Jiang *et al.*, 2012). The consequence of this may be that TM1 and TM2 move away from the central axis by ~3 Å to expand the ion conductive pore (Khakh and North, 2012). However, the molecular dynamics simulation of the hP2X3 receptor in the absence of any ligand was compatible with the assumption that the ectodomain movement in the binding pouch occurs in the absence of its agonist. Thus, the approaching of beak and dorsal fin of adjacent receptor subunits in hP2X3 receptors could be a spontaneous intermediate step for receptor activation or receptor desensitization.

By using an rP2X2-X1 chimera, it was previously shown that ATP dissociates more slowly from the open state than from the closed state of the rP2X2-X1 chimera (Bongartz *et al.*, 2010). For the mouse muscle acetylcholine receptor ($\alpha_2\beta\delta\varepsilon$ AChR), it was calculated/predicted that di-liganded activation bursts are more likely to be terminated by ACh dissociation from the closed state AChR than from the open or desensitized state of the AChR (Grosman and Auerbach, 2001), thus indicating that ACh dissociates more slowly from the open or desensitized state in comparison to the closed state of the AChR. Also, analysis of single channel recordings of AChR mutants was instrumental to estimate that the affinity for ACh is markedly greater for the open conformation than for the closed conformation of the AChR (Purohit and Auerbach, 2009). We thus hypothesize that the jaw closure of the ATP binding site, besides its role in channel gating (Hattori and Gouaux, 2012; Jiang *et al.*, 2012; Lörinczi *et al.*, 2012), may also decelerate the agonist dissociation from the open state and thus increase the agonist affinity of the open state of the hP2X3 receptor. However, because in the hP2X3 receptor the inactivation kinetics are dominated by the fast desensitization, the experimental verification of this hypothesis is difficult.

An important question relates to the issue whether the hP2X3 receptor cysteine double mutants, responding to α,β-meATP with only negligible current amplitudes, were expressed as trimeric proteins in the plasma membrane, or whether they were retained in the cell interior due to misassembly and/or incomplete trafficking. Biochemical analysis of His-tagged hP2X3 receptor mutants confirmed the expression at the plasma membrane and revealed under non-denaturing conditions the existence of a protein consisting of three subunits linked to each other by disulfide bonds. Under reducing conditions (presence of DTT), the homotrimeric receptor-protein was disintegrated into its protomers.

Our results obtained in the *X. laevis* oocyte expression system have shown that the DTT-mediated modulation of the current amplitudes, the plasma membrane expression and the oligomer formation is similar in HEK293 cells and oocytes, indicating that our results are independent of the expression system used. Furthermore, biochemical analysis of oocyte- and HEK293 cell-expressed hP2X3 proteins demonstrated that the analysed mutations did not interfere with assembly and plasma membrane trafficking in either system, indicating that the functional impairment of certain mutants was due to affected ligand binding or channel gating. The BN-PAGE data perfectly show that the mutants appear at the cell surface in a disulfide cross-linked homotrimeric state.

Cysteine double mutants such as M200C/V274C-hP2X3 that showed no change of the α,ß-meATP-evoked current after DTT treatment were as fully cross-linked as the K201C/V274C-hP2X3 mutant, which exhibited the most pronounced increase of the current response following DTT treatment. This finding indicates that it is not the disulfide bond *per se* that impairs the function, but its specific position. The biochemically demonstrated disulfide bond formation of all the cysteine double mutants examined strongly indicates that the substituted two cysteine residues must be in close spatial vicinity of <4.6 Å in the closed state of the receptor; this is the maximum distance between the C_β-carbons of cysteines that can be bridged by a disulfide bond (Careaga and Falke, 1992; see our molecular modelling data). The variation in the level of functional impairment indicates that some positions are more sensitive for conformational fixation than others; in other words, conformational movement or flexibility of specific positions, such as K201C/V274C of the hP2X3 receptor are an essential prerequisite for agonist binding and/or channel gating of the hP2X3 receptor. Possibly, the transduction of the closed state to the agonist-bound open state of the hP2X3 receptor is not a predetermined sequence of mutually dependent steps of conformational changes, but also depends upon the random occurrence of intermediate steps, which require conformational flexibility.

BODIPY ATP has been used, for example, for imaging exocytosis from ATP-containing vesicles (Akopova *et al.*, 2012) or for determining ATP binding to P-glycoprotein transporters (Alcantara *et al.*, 2013). Most likely BODIPY ATP indiscriminately occupies binding sites of various types of ATP binding proteins present in the plasma membrane. However, these sites (see also the catalytic domains of class II aminoacyl-tRNA synthetases) might be unrelated to those of P2X receptors (Freist *et al.*, 1998; Mager *et al.*, 2004). In view of the dramatic differences in the fluorescence intensity between K113C/K201C-hP2X3 and K201C/V274C-hP2X3, we suggest that at the former mutant, the introduction of the respective disulfide bonds inhibits predominantly gating,

whereas at the latter mutant, agonist binding was hindered by the disulfide bond.

In conclusion, we have shown that the mutant receptor K113C/K201C-hP2X3 (and possibly also E112C/R198C- and K113C/R198C-hP2X3) exhibit spontaneous formation of inter-subunit cross links, confirming our hypothesis that a spontaneous tightening of the binding jaw of the hP2X3 receptor at AA positions not involved in agonist binding occurs without altering binding, subunit assembly or trafficking behaviour. A high conformational mobility of beak and dorsal fin of adjacent subunits in hP2X3 receptors is supposed to be a prerequisite for agonist binding and receptor activation.

Acknowledgements

We are grateful to Mr Nick Helms (Rudolf-Boehm-Institute of Pharmacology and Toxicology, University of Leipzig, Leipzig, Germany), Drs Lars Thomas and Alexander Vogel (both from the Institute of Medical Physics and Biophysics, University of Leipzig, Leipzig, Germany) for methodological help. We thank Mrs Ursula Braam (Department of Molecular Pharmacology, RWTH Aachen University, Aachen, Germany) for the generation of the HEK 293 Tet-on stable cell lines, cell culturing and assistance in the generation of hP2X3 mutants. The financial support of the Deutsche Forschungsgemeinschaft (RI 2092/1-2, IL 20/18-2, HA 6095/1 and Schm 536/8) is gratefully acknowledged. We thank Professor Yu Ye (Shanghai Institutes for Biological Sciences, Chinese Academy of Sciences, Shanghai, China) for helpful discussions on the molecular dynamics data.

Author contributions

M. K., R. H., G. S., P. I. and T. R. conceived and designed the experiments. M. K., R. H., M. G. and A. D. performed the experiments. M. K., R. H., H. F., K. N. and T. R. analysed the data. M. K., R. H., H. F., G. S., P. I. and T. R. wrote the manuscript. R. H., H. F., K. N., G. S., P. I. and T.R. contributed financial support/reagents/materials/analysis tools. M. K., R. H., G. S., P. I. and T.R. drafted and edited the manuscript.

Conflict of interest

None.

References

Abbracchio MP, Burnstock G (1994). Purinoceptors: are there families of P2X and P2Y purinoceptors? Pharmacol Ther 64: 445–475.

Agboh KC, Powell AJ, Evans RJ (2009). Characterisation of ATP analogues to cross-link and label P2X receptors. Neuropharmacology 56: 230–236.

Alexander SPH, Benson HE, Faccenda E, Pawson AJ, Sharman JL, Catterall WA *et al.* (2013a). The Concise Guide to PHARMACOLOGY 2013/14: Ligand-Gated Ion Channels. Br J Pharmacol 170: 1582–1606.

Alexander SPH, Benson HE, Faccenda E, Pawson AJ, Sharman JL Spedding M *et al.* (2013b). The Concise Guide to PHARMACOLOGY 2013/14: G Protein-Coupled Receptors. Br J Pharmacol 170: 1459–1581.

Akopova I, Tatur S, Grygorczyk M, Luchowski R, Gryczynski I, Gryczynski Z *et al.* (2012). Imaging exocytosis of ATP-containing vesicles with TIRF microscopy in lung epithelial A549 cells. Purinergic Signal 8: 59–70.

Alcantara LM, Kim J, Moraes CB, Franco CH, Franzoi KD, Lee S *et al.* (2013). Chemosensitization potential of P-glycoprotein inhibitors in malaria parasites. Exp Parasitol 134: 235–243.

Allsopp RC, El Ajouz S, Schmid R, Evans RJ (2011). Cysteine scanning mutagenesis (residues Glu52-Gly96) of the human P2X1 receptor for ATP: mapping agonist binding and channel gating. J Biol Chem 286: 29207–29217.

Aschrafi A, Sadtler S, Niculescu C, Rettinger J, Schmalzing G (2004). Trimeric architecture of homomeric P2X2 and heteromeric P2X1+2 receptor subtypes. J Mol Biol 342: 333–343.

Bhargava Y, Nicke A, Rettinger J (2013). Validation of Alexa-647-ATP as a powerful tool to study P2X receptor ligand binding and desensitization. Biochem Biophys Res Commun 438: 295–300.

Bodnar M, Wang H, Riedel T, Hintze S, Kató E, Fallah G *et al.* (2011). Amino acid residues constituting the agonist binding site of the human P2X3 receptor. J Biol Chem 286: 2739–2749.

Bongartz EV, Rettinger J, Hausmann R (2010). Aminoglycoside block of P2X2 receptors heterologously expressed in *Xenopus laevis* oocytes. Purinergic Signal 6: 393–403.

Burnstock G, Wood JN (1996). Purinergic receptors: their role in nociception and primary afferent neurotransmission. Curr Opin Neurobiol 6: 526–532.

Careaga CL, Falke JJ (1992). Structure and dynamics of *Escherichia coli* chemosensory receptors. Engineered sulfhydryl studies. Biophys J 62: 209–216.

Clyne JD, Wang LF, Hume RI (2002). Mutational analysis of the conserved cysteines of the rat P2X2 purinoceptor. J Neurosci 22: 3873–3880.

Egan TM, Cox JA, Voigt MM (2004). Molecular structure of P2X receptors. Curr Top Med Chem 4: 821–829.

Ennion SJ, Evans RJ (2002). Conserved cysteine residues in the extracellular loop of the human P2X1 receptor form disulfide bonds and are involved in receptor trafficking to the cell surface. Mol Pharmacol 61: 303–311.

Fallah G, Romer T, Detro-Dassen S, Braam U, Markwardt F, Schmalzing G (2011). TMEM16A(a)/anoctamin-1 shares a homodimeric architecture with CLC chloride channels. Mol Cell Proteomics 10: M110.

Fiser A, Sali A (2003). Modeller: generation and refinement of homology-based protein structure models. Methods Enzymol 374: 461–491.

Freist W, Verhey JF, Stühmer W, Gauss DH (1998). ATP binding site of P2X channel proteins: structural similarities with class II aminoacyl-tRNA synthetases. FEBS Lett 434: 61–65.

Grosman C, Auerbach A (2001). The dissociation of acetylcholine from open nicotinic receptor channels. Proc Natl Acad Sci U S A 98: 14102–14107.

Hattori M, Gouaux E (2012). Molecular mechanism of ATP binding and ion channel activation in P2X receptors. Nature 485: 207–212.

Hausmann R, Rettinger J, Gerevich Z, Meis S, Kassack MU, Illes P *et al.* (2006). The suramin analog 4,4′,4″,4‴-(carbonylbis (imino-5,1,3-benzenetriylbis (carbonylimino)))tetra-kis-benzenesulfonic acid (NF110) potently blocks P2X3 receptors: subtype selectivity is determined by location of sulfonic acid groups. Mol Pharmacol 69: 2058–2067.

Hausmann R, Bodnar M, Woltersdorf R, Wang H, Fuchs M, Messemer N *et al.* (2012). ATP binding site mutagenesis reveals different subunit stoichiometry of functional P2X2/3 and P2X2/6 receptors. J Biol Chem 287: 13930–13943.

Hausmann R, Günther J, Kless A, Kuhlmann D, Kassack MU, Bahrenberg G *et al.* (2013). Salt bridge switching from Arg290/Glu167 to Arg290/ATP promotes the closed-to-open transition of the P2X2 receptor. Mol Pharmacol 83: 73–84.

Jiang LH, Rassendren F, Surprenant A, North RA (2000). Identification of amino acid residues contributing to the ATP-binding site of a purinergic P2X receptor. J Biol Chem 275: 34190–34196.

Jiang R, Martz A, Gonin S, Taly A, de Carvalho LP, Grutter T (2010). A putative extracellular salt bridge at the subunit interface contributes to the ion channel function of the ATP-gated P2X2 receptor. J Biol Chem 285: 15805–15815.

Jiang R, Lemoine D, Martz A, Taly A, Gonin S, Prado de Carvalho L *et al.* (2011). Agonist trapped in ATP-binding sites of the P2X2 receptor. Proc Natl Acad Sci U S A 108: 9066–9071.

Jiang R, Taly A, Lemoine D, Martz A, Cunrath O, Grutter T (2012). Tightening of the ATP-binding sites induces the opening of P2X receptor channels. EMBO J 31: 2134–2143.

Jiang R, Taly A, Grutter T (2013). Moving through the gate in ATP-activated P2X receptors. Trends Biochem Sci 38: 20–29.

Károly R, Mike A, Illes P, Gerevich Z (2008). The unusual state-dependent affinity of P2X3 receptors can be explained by an allosteric two-open-state model. Mol Pharmacol 73: 224–234.

Kaczmarek-Hájek K, Lörinczi E, Hausmann R, Nicke A (2012). Molecular and functional properties of P2X receptors – recent progress and persisting challenges. Purinergic Signal 8: 375–417.

Kawate T, Michel JC, Birdsong WT, Gouaux E (2009). Crystal structure of the ATP-gated P2X4 ion channel in the closed state. Nature 460: 592–598.

Khakh BS, North RA (2012). Neuromodulation by extracellular ATP and P2X receptors in the CNS. Neuron 76: 51–69.

Liang X, Xu H, Li C, Yin S, Xu T, Liu J *et al.* (2013). Functional identification of close proximity amino acid side chains within the transmembrane-spanning helixes of the P2X2 receptor. PLoS ONE 8: e70629.

Lörinczi E, Bhargava Y, Marino SF, Taly A, Kaczmarek-Hajek K, Barrantes-Freer A *et al.* (2012). Involvement of the cysteine-rich head domain in activation and desensitization of the P2X1 receptor. Proc Natl Acad Sci U S A 109: 11396–11401.

Mager PP, Weber A, Illes P (2004). Bridging the gap between structural bioinformatics and receptor research: the membrane-embedded, ligand-gated, P2X glycoprotein receptor. Curr Top Med Chem 4: 1657–1705.

Marquez-Klaka B, Rettinger J, Bhargava Y, Eisele T, Nicke A (2007). Identification of an intersubunit cross-link between substituted cysteine residues located in the putative ATP binding site of the P2X1 receptor. J Neurosci 27: 1456–1466.

Marquez-Klaka B, Rettinger J, Nicke A (2009). Inter-subunit disulfide cross-linking in homomeric and heteromeric P2X receptors. Eur Biophys J 38: 329–338.

Nagaya N, Tittle RK, Saar N, Dellal SS, Hume RI (2005). An intersubunit zinc binding site in rat P2X2 receptors. J Biol Chem 280: 25982–25993.

Nicke A, Baumert HG, Rettinger J, Eichele A, Lambrecht G, Mutschler E *et al.* (1998). P2X1 and P2X3 receptors form stable trimers: a novel structural motif of ligand-gated ion channels. EMBO J 17: 3016–3028.

North RA (2002). Molecular physiology of P2X receptors. Physiol Rev 82: 1013–1067.

Pawson AJ, Sharman JL, Benson HE, Faccenda E, Alexander SP, Buneman OP, Davenport AP, McGrath JC, Peters JA, Southan C, Spedding M, Yu W, Harmar AJ; NC-IUPHAR. (2014). The IUPHAR/BPS Guide to PHARMACOLOGY: an expert-driven knowledge base of drug targets and their ligands. Nucl. Acids Res. 42 (Database Issue): D1098–1106.

Petrenko N, Khafizov K, Tvrdonova V, Skorinkin A, Giniatullin R (2011). Role of the ectodomain serine 275 in shaping the binding pocket of the ATP-gated P2X3 receptor. Biochemistry 50: 8427–8436.

Purohit P, Auerbach A (2009). Unliganded gating of acetylcholine receptor channels. Proc Natl Acad Sci U S A 106: 115–120.

Riedel T, Schmalzing G, Markwardt F (2007). Influence of extracellular monovalent cations on pore and gating properties of P2X7 receptor-operated single-channel currents. Biophys J 93: 846–858.

Riedel T, Wiese S, Leichsenring A, Illes P (2012). Effects of nucleotide analogs at the P2X3 receptor and its mutants identify the agonist binding pouch. Mol Pharmacol 82: 80–89.

Roberts JA, Digby HR, Kara M, El Ajouz S, Sutcliffe MJ, Evans RJ (2008). Cysteine substitution mutagenesis and the effects of methanethiosulfonate reagents at P2X2 and P2X4 receptors support a core common mode of ATP action at P2X receptors. J Biol Chem 283: 20126–20136.

Roberts JA, Valente M, Allsopp RC, Watt D, Evans RJ (2009). Contribution of the region Glu181 to Val200 of the extracellular loop of the human P2X1 receptor to agonist binding and gating revealed using cysteine scanning mutagenesis. J Neurochem 109: 1042–1052.

Roberts JA, Allsopp RC, El Ajouz S, Vial C, Schmid R, Young MT *et al.* (2012). Agonist binding evokes extensive conformational changes in the extracellular domain of the ATP-gated human P2X1 receptor ion channel. Proc Natl Acad Sci U S A 109: 4663–4667.

Rokic MB, Tvrdonova V, Vavra V, Jindrichova M, Obsil T, Stojilkovic SS *et al.* (2010). Roles of conserved ectodomain cysteines of the rat P2X4 purinoreceptor in agonist binding and channel gating. Physiol Res 59: 927–935.

Wirkner K, Sperlagh B, Illes P (2007). P2X3 receptor involvement in pain states. Mol Neurobiol 36: 165–183.

Supporting information

Additional Supporting Information may be found in the online version of this article at the publisher's web-site:

http://dx.doi.org/10.1111/bph.12830

Figure S1 Cysteine mutagenesis for analysing relevance of ectodomain movement for receptor behaviour. (A) Homology model of the hP2X3 receptor with its three receptor subunits coloured in white, light blue and black, based upon the closed zfP2X4R crystal structure. (B) One P2X3 receptor subunit shown in a dolphin-like shape with positions of cysteine mutants. (C) Cysteine double mutants cross-link adjacent receptor subunits at varying positions via an inter-subunit disulfide bond (a, inter-subunit: beak and dorsal fin; b, inter-subunit: dorsal fin and left flipper; c, intra-subunit: beak and left flipper). (D) List of the investigated cysteine double mutants enabling the generation of a disulfide bond between the above-mentioned domains.

Figure S2 Homology model of the hP2X3 receptor based upon the open zfP2X4R crystal structure. (A) The beak-dorsal fin interface is shown with beak residues Glu-111, Glu-112, Lys-113, Glu-125 and Arg-126 and the dorsal fin residues Arg-198 and Lys-201. (B) The dorsal fin-left flipper interface is shown with dorsal fin residues Met-200 and Lys-201 and the left flipper residue Val-274. (C) The beak-left flipper interface is shown with beak residue Lys-113 and left flipper residue Glu-270.

Figure S3 Reversibility of disulfide bond formation in the cysteine single and double mutant hP2X3 receptors expressed in HEK293 cells by DTT. (A) Molecular models of the three cysteine double mutant hP2X3 receptors K113C/K201C (cross-linking beak/dorsal fin; Aa), M200C/V274C and K201C/V274C (cross-linking dorsal fin/left flipper; Ab, c) of adjacent receptor subunits with the bound agonist ATP and the introduced disulfide bonds. We assume that the disulfide bonds are not accessible to DTT in case of the M200C/V274C mutation. (B) Additional DTT-reversibility protocol shown for the hP2X3 receptor mutants K113C/K201C and K201C/V274C (the last 5 min of DTT incubation is in the absence of any agonist application), for checking disulfide bond formation in the absence of α,β-meATP.

Figure S4 Function, cell surface expression and assembly of the hP2X3 receptor and its mutants in *X. laevis* oocytes. (A) Shown are original current traces from oocytes expressing the indicated hP2X3 mutants. Currents were elicited by 5 s applications of 10 μM α,β-meATP (indicated by the short horizontal bars) in 5 min intervals before, during and after application of 1 mM DTT (presence of DTT indicated by the grey box). (B) The bars show the mean ± SEM of the current amplitudes (n = 5–7) of the indicated hP2X3 construct. The data were calculated by normalizing the maximal or minimal current amplitude during or following exposure to DTT, respectively, to the mean current amplitude prior to exposure to DTT. *P < 0.05, significant changes in the current amplitudes by DTT exposure. (C, panels a–c) The plasma membrane-bound form of the indicated hP2X3 mutants was covalently labelled with IR800, purified by Ni-NTA chromatography, resolved by non-reducing and reducing SDS-PAGE and visualized by fluorescence scanning. Note that the non-reduced hP2X3 cysteine single mutants migrated almost exclusively as monomers (C, panels a, c), while the non-reduced double mutants migrated as oligomers, most likely homotrimers (C, panels b, c). (D, panels a–c) The indicated plasma membrane-bound hP2X3 proteins were resolved by BN-PAGE both in the non-denatured state and after partial denaturation following a 1 h incubation with SDS and/or DTT at 37°C. Note that the trimeric forms of the wt and cysteine single mutants dissociated in 0.1% SDS into dimers and monomers, while the trimeric form of the cysteine double mutants required reduction of disulfide bonds by DTT in addition to SDS to dissociate. The ovals in the left margins indicate the numbers of hP2X3 subunits incorporated in the respective protein band.

Figure S5 Visualization of agonist binding using BODIPY-TR ATP (BODIPY ATP). (A) Comparison of the effect of ORi (oocyte Ringer's solution) and 1 mM DTT dissolved in ORi on the background fluorescence of *X. leavis* oocytes expressing hP2X3-wt at time zero. Laser scanning confocal microscopy was used as shown in Figure 6. Each column indicates the mean ± SEM of five oocytes. (B) The fluorescence intensity of 1 μM BODIPY ATP (a), 1 mM DTT plus 1 μM BODIPY ATP (b) and 1 mM DTT (c) was recorded with a fluorescence spectrometer (excitation maximum at 592 nm and emission spectrum from 600 to 650 nm). One representative experiment out of three similar ones.

Table S1 Analysis of the distance between pairs of cysteine double mutants of the closed hP2X3 receptor structure (on which our molecular dynamics simulation is based) as compared with the open hP2X3 receptor structure, both based upon the zfP2X4 receptor. The inter-cysteine distances were determined at the backbone of the hP2X3 receptor and are shown in Å between the C_α-carbons. The three groups of cysteine double mutants separated by broken lines are those cross-linking beak/dorsal fin, beak/left flipper and dorsal fin/left flipper respectively.